Q. J. R. Meteorol. Soc. (2000), **126**, pp. 991–1029

The second COMPARE exercise: A model intercomparison using a case of a typical mesoscale orographic flow, the PYREX IOP3

By MARC GEORGELIN[1]*, PHILIPPE BOUGEAULT[2]†, THOMAS BLACK[3], NEDJLEJKA BRZOVIC[4], ANDREA BUZZI[12], JAVIER CALVO[5], VINCENT CASSÉ[2], MICHEL DESGAGNÉ[6], RYAD EL-KHATIB[2], JEAN-FRANCOIS GELEYN[2], TEDDY HOLT[7], SONG-YOU HONG[3], TERUYUKI KATO[8], JACK KATZFEY[13], KAZUO KURIHARA[9], BRUNO LACROIX[2], FRANCOIS LALAURETTE[10], YVON LEMAITRE[2], JOCELYN MAILHOT[6], DETLEV MAJEWSKI[11], PIETRO MALGUZZI[12], VALERY MASSON[2], JOHN McGREGOR[13], ENRICO MINGUZZI[14], TIZIANA PACCAGNELLA[14] and CLIVE WILSON[15]

[1]*Laboratoire d'Aérologie, Université Paul Sabatier, France*
[2]*Centre National de Recherche Météorologiques, France*
[3]*National Centers for Environmental Prediction, USA*
[4]*Meteorological and Hydrological Service, Croatia*
[5]*Instituto Nacional de Meteorologia, Spain*
[6]*Recherche en Prévision Numérique, Atmospheric Environment Service, Canada*
[7]*Naval Research Laboratory, USA*
[8]*Meteorological Research Institute, Japan*
[9]*Japan Meteorological Agency, Japan*
[10]*European Centre for Medium-Range Weather Forecasts, UK*
[11]*Deutscher Wetterdienst, Germany*
[12]*National Research Council of Italy FISBAT Institute, Italy*
[13]*Commonwealth Scientific and Industrial Research Organisation, Australia*
[14]*Servizio Meteorologico Regionale de Emilia Romagna, Italy*
[15]*The Met. Office, UK*

(Received 29 May 1998; revised 23 March 1999)

SUMMARY

Fifteen models have been evaluated for their ability to simulate the various phenomena of a mesoscale orographic flow sampled during the Pyrénées experiment (PYREX). A pure forecast exercise has been conducted and model performances were assessed using numerous observations. Two additional experiments were also performed in order to discriminate between small-scale errors and large-scale induced errors, and to discuss an optimal specification of model terrain height and roughness for use with envelope orography and effective roughness length parametrizations.

The comparison results reveal systematic errors for all the models: the local winds are too weak, the mountain-wave amplitude is too large and the lee vortices are poorly represented. Since forcing by analyses did not correct the errors, they can be therefore mainly attributed to the model representation of orography. The blocking created by the model topography at low level is under-represented and the model topography does not sufficiently slow the flow.

A positive consequence of the effective roughness length parametrization is to reduce the mountain-wave amplitude. Negligible benefit occurs from the use of an envelope orography parametrization. Although it favours the appearance of the lee vortices, the latter appear too early, the local winds remain too weak, and the mountain-wave amplitude is enhanced. The comparison of the computed pressure drag with the observed one is reasonably good for most of the models but the pressure drag is found to be more correlated to the lee vorticity than to the mountain wave.

KEYWORDS: Effective roughness length Envelope orography Local winds Mesoscale Model intercomparison Mountain wave Pressure drag

1. THE COMPARE PROGRAMME

The COMPARE (Comparison of Mesoscale Prediction and Research Experiment) project has been set up by the Working Group on Numerical Experimentation (WGNE) of the Commission of Atmospheric Science (World Meteorological Organization) in order to develop scientifically sound methods of intercomparisons of results of mesoscale

* Deceased September 1999.
† Corresponding author: Centre National de Recherche Météorologiques, Météo-France, 42, Avenue G. Coriolis, 31057 Toulouse, France.

models, and address key issues on the formulation of these models in relation to specific forecasting problems.

It is intended as a long term project, with the objective of putting together an ever increasing set of well-documented cases, using a common format of analyses and forecasts, which are available to any group involved in the development and validation of mesoscale numerical models. These cases are taken from major field experiments in order to ensure the best possible quality of the distributed data. They are proposed by various sponsors, offering to support the technical work involved in the distribution of data and analysis of results, for the common benefit.

COMPARE is supervised by a steering group whose responsibilities are: (i) to select the cases, (ii) to ensure the availability of data and resources necessary to prepare the distribution of analyses and to evaluate the results, (iii) to design the set of experiments proposed to the participants, (iv) to guarantee their suitability to address the scientific issues of interest for each case, (v) to review the scientific conclusions of each exercise.

The first intercomparison exercise to be run under the auspices of the COMPARE project concerned a typical explosive marine cyclogenesis observed during the Canadian Atlantic Storms Project (CASP) field experiment (Gyakum *et al.* 1995, 1996). The present paper summarizes the results obtained during the second exercise, sponsored by the Centre National de Recherche Météorologiques (CNRM). It concerns a typical example of orographic flow observed during the Pyrénées experiment (PYREX). The numerical simulations were run during 1995–1996 and the present results were discussed among the participants during the COMPARE/PYREX workshop held in Toulouse, France, on 3–5 September 1996.

2. Presentation of the COMPARE/PYREX exercise

(*a*) *Summary of orographic flows and PYREX*

In this section we introduce the main concepts and terminology used for the interpretation of the experiments.

In orographic flows, the behaviour of an air parcel depends strongly on its initial altitude. The lowest layers of the troposphere rarely have enough energy to cross obstacles the height of a mountain; the air is thus diverted on each side of the orographic barrier, and the flow is mainly horizontal. The two flows going around the mountain at low level are known as local winds. A study of this mechanism can be found in Koffi *et al.* (1997) who show the ability of the linear theory to represent local winds in a configuration close to the one found in the Pyrénées. Some case studies of local winds existing in the vicinity of the Pyrénées may be found in Campins *et al.* (1995), Masson and Bougeault (1996), Georgelin *et al.* (1996).

The point upwind where the flow separates into two branches is the separation (or saddle) point. In the centre of the ridge there is a stagnation point which, in fact, separates the flow above from the flow around the barrier. This theoretical point corresponds to a zone where the wind is very weak and is called the blocking zone. Below this zone, the flow has no other course but to flow backward into the centre of the obstacle and around it on each side. Figure 1, derived from the work of Olafsson and Bougeault (1996) shows a (realistic) low-Froude number flow impinge on an elliptical obstacle, representative of the Pyrénées case. The Froude number is defined as U/NH where U is the upstream flow speed, N the Brunt–Vaisala (buoyancy) frequency and H the height of the mountain. The location of the blocking zone and the separation point are indicated.

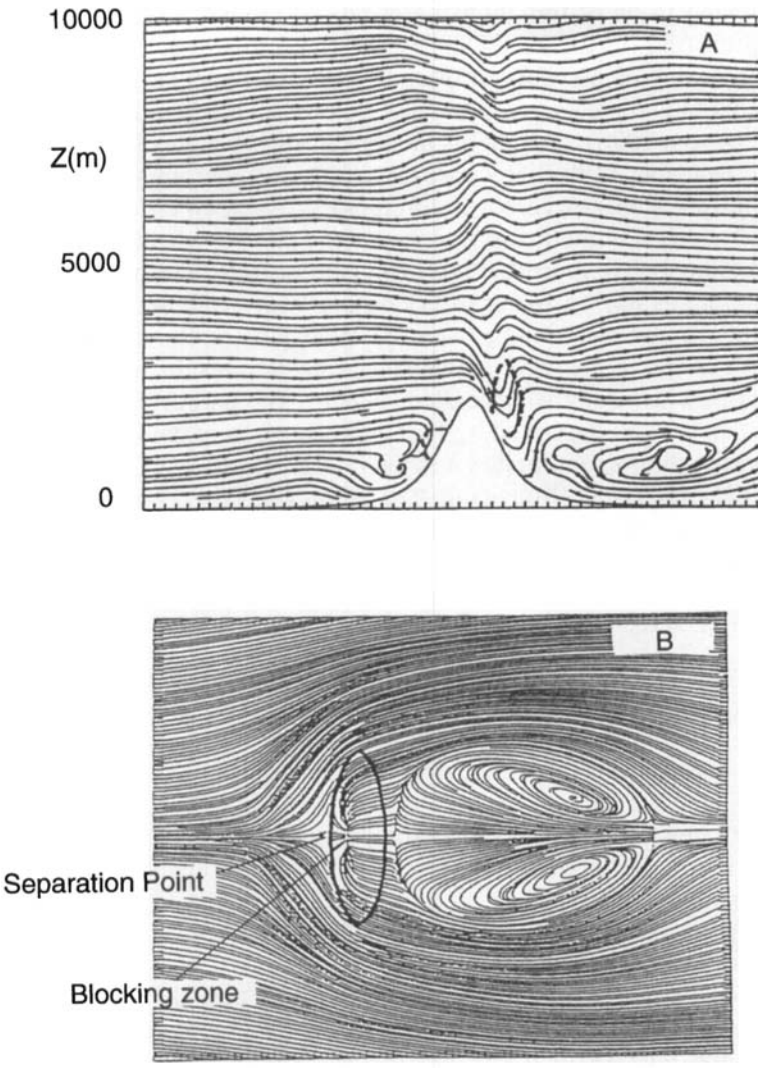

Figure 1. Theoretical view of a mesoscale orographic flow for an inverse Froude number $(NH/U) = 2.273$ (adapted from Olafsson and Bougeault 1996). (A) Streamlines on a cross-mountain vertical section; (B) streamlines at first model level.

Downwind from the mountain, a wake is created in the form of two symmetrical and counter-rotative vortices. Numerous observations of such vortices exist, for example see Smith and Grubišić (1993). Such lee vortices are of great interest to the research community, especially regarding the way they are created (viscous versus inviscid mechanisms), and the way potential vorticity is created by the cumulative dissipation in the wake, (Schär and Durran 1997; Smolarkiewicz and Rotunno 1989). The part of the flow which goes around the mountain can be therefore characterized by three main aspects: the blocking, the local winds and the wake vortices.

The higher layers of the atmosphere can cross the mountain and because the troposphere is stably stratified, the buoyancy restoring forces give rise to internal gravity waves which propagate vertically, known as mountain waves. It can be demonstrated that these topographic waves transport energy upward and momentum downward. In

the linear case the value of this momentum flux at ground level compensates for the pressure drag exerted on the mountain by the flow; this drag can be calculated and its value is a measure of the wave amplitude. The real flows are in general non-linear and so the mountain wave system does not behave as predicted by the linear theory (Smith 1989; Durran 1990), though this theory can still be a good predictor for the drag (Olafsson and Bougeault 1997). Because the mountains are rough and the process non-linear, the atmosphere is slowed down during the crossing of the obstacle and thus the vertical profile of momentum flux is divergent at the altitude where the slowdown occurs (Eliassen and Palm 1960). Indeed, it has been demonstrated during the last decade that mesoscale mountains have a major effect on the large-scale atmospheric circulation. Downwind, the air parcels coming from the other side of the mountain, undergo an adiabatic compression in the wave movement. A heating results from this compression which often goes with strong winds called 'Foehn'. The part of the flow which crosses the mountain can be well described by four aspects: the mountain wave shape, its drag, the vertical profile of momentum flux and the Foehn effect.

The PYREX experiment (Bougeault *et al.* 1990, 1993, 1997) was a joint programme of Météo-France and the Spanish Meteorological Institute, with the participation of several research institutes and funding agencies of France, Spain, and Germany. Its objective was to measure various contributions to the momentum budget of the flow over the Pyrénées, at the mesoscale. The measurements included:

- Surface parameters by 15 automatic weather stations, placed at high elevations along the central transect, including high accuracy pressure measurements, from which it was possible to compute the drag in near real-time.
- Radio-soundings at 11 stations, 4 times a day during the Intensive Observation Periods (IOP).
- A network of 4 wind profilers, operating continuously along the central transect.
- Trajectories of constant-level balloons, both along the central transect, and around the eastern edge of the range.
- Surface measurements by a large number (over 100) of weather stations, and by 5 sodars in the domain of the main regional winds.
- Mean and turbulent dynamic and thermodynamic measurements taken from four instrumented aircraft, flying over the main transect and around the eastern edge.
- An airborne lidar system allowing for the remote detection of clouds and the planetary boundary layer depth.

The third intensive observation period (14–15 October 1990), selected for the second COMPARE exercise, features a typical, strong lee wave event, with a brief (few hours) peak of surface pressure drag and wave momentum flux. This is associated with significant surface flow perturbations which are of interest for regional forecasts. The following is a summary of this case; a more complete description may be found in Bougeault *et al.* (1993).

Although the wind, at the synoptic scale, had been oriented south-west of the area of interest for several days, the situation became most favourable for strong mountain waves only in the evening of 14 October, due to the approach of a trough over the eastern Atlantic. This is shown by the 500 hPa wind field in Fig. 2, valid at 0000 UTC, 15 October. This trough directed south to south-westerly winds over the Pyrénées, with intensity reaching 15 m s^{-1} at 700 hPa, 20 m s^{-1} at 500 hPa, and 40 m s^{-1} at the tropopause, just above 200 hPa. During the whole IOP, the core of the wind maximum was drifting slowly to the east, resulting in conditions of maximum low-level winds in the morning of 15 October, when the aircraft mission took place.

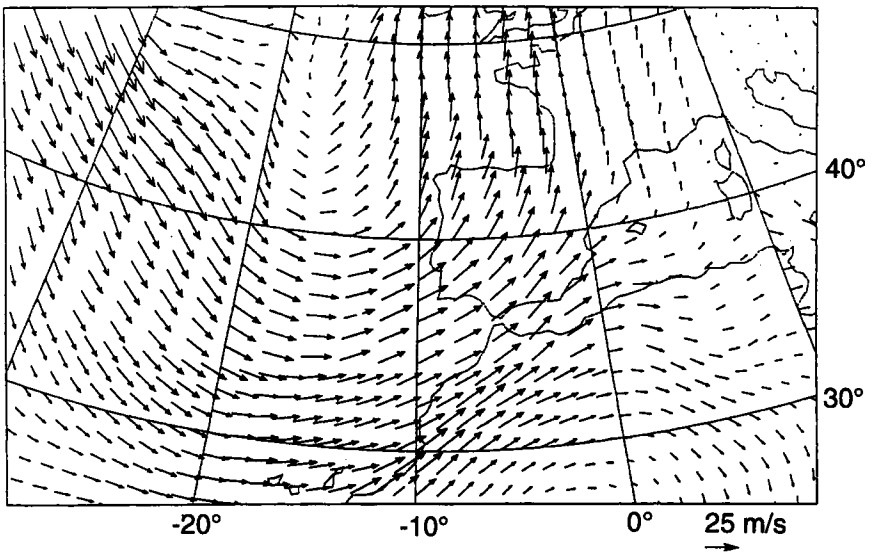

Figure 2. The 500 hPa wind on 15 October, 00 UTC in the area of interest.

The Foehn effect started during the night on the northern side of the range, leading to a spectacular time evolution of temperature and humidity at several stations in the foothills. The onset occurred early in the night on the western side, near midnight in the centre of the range, and late in the night on the eastern side, suggesting that the Foehn followed the eastward drift of the large-scale system. The temperature in the foothills rose to unusual values on the morning of 15 October, whereas moisture was at a low 40%. The wind at some of the foothills stations also reached some significant values, with a maximum gust of 16 m s^{-1} from the south of Lannemezan, Central Pyrénées.

At the peak intensity of the event, during the morning, a full description of the mountain wave is available from three aircraft flying simultaneously. This includes unique measurements of turbulence at very low levels above, and in the wake of, the range. The wave momentum flux has been computed for several altitudes, and the pressure drag across the range during the whole period is also available.

During the whole period, the area of Toulouse was subject to the classical 'Autan' wind, reaching a force of about 15 m s^{-1}. This wind usually occurs in connection with synoptic flow from the south-west and is limited to a shallow layer below a strong inversion. This has been documented by the fourth research aircraft, giving the three-dimensional structure of the strong wind tube. Other places in the PYREX area had very weak winds, due to a shelter effect.

Finally, one of the most interesting aspects of the surface wind field is the formation in the early afternoon of 15 October of a small-scale lee vortex pair (about 100 km in diameter). These vortices also drifted slowly towards the west, and were documented by the surface meso-network, and by the Lannemezan Sodar.

The event intensity decreased during the afternoon, whereas the south-west flow was still present at altitude.

In addition, synopticians noted a frontal system embedded in the trough, producing some clouds over the ocean and upstream of the Pyrénées. The front reached the western edge of the mountain ridge near 1200 UTC, 15 October, and it probably continued to propagate eastward through the experimental area. However, there is

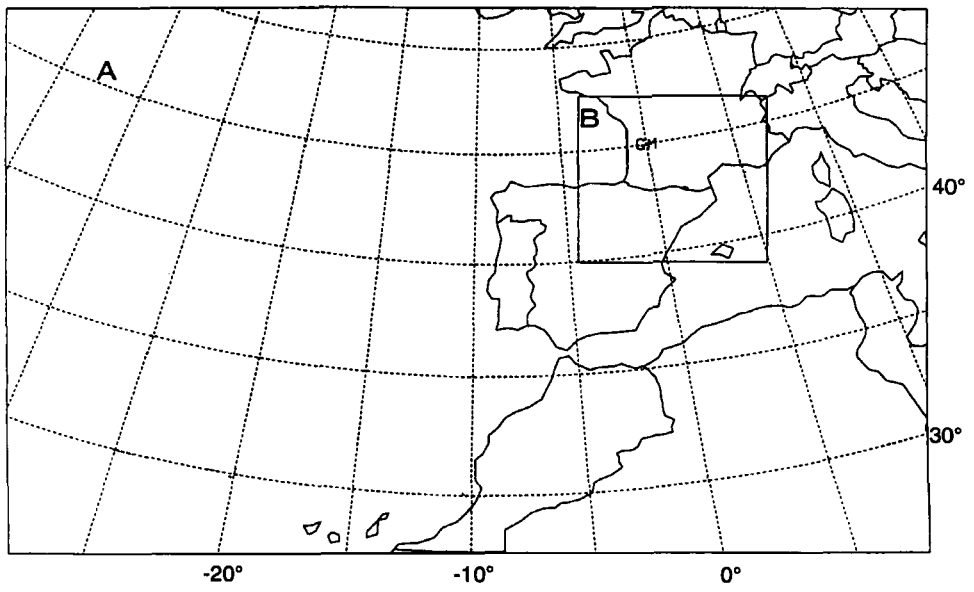

Figure 3. Domains for the study.

hardly any evidence of its passage during subsequent hours, and we assume that it was progressively dissolving.

(*b*) *Numerical experiments*

The first issue put forward during the definition phase of the exercise was to verify that the models are able to simulate the whole sequence of events described above, seen as the local response to a slowly varying synoptic flow. In particular, the formation and destruction of the lee vortices at the correct time, and also the history of the surface pressure drag and wave momentum flux was considered to be an interesting test for the models.

A second issue was to discriminate between the large-scale errors and the small-scale errors in the production of wrong forecasts. This called for extensive comparisons between experiments where the large-scale part of the flow is continuously relaxed towards the analyses (dynamical adaptation) and actual forecasts.

Finally, one key question concerning orographic flows was the optimal specification of the model terrain height and roughness. Recent work by the PYREX group (Bougeault *et al.* 1992; Georgelin *et al.* 1994) had illustrated the benefits of taking into account the subgrid-scale orography by increasing both the terrain height (envelope orography) and the roughness. On the other hand, it was felt necessary to test each model with its usual specification of orography and roughness because of possible implicit representation of these aspects by other parts of the model physics.

Figure 3 shows the various domains for the study. Following the protocol proposed by Chouinard *et al.* (1994), Domain A has been designed to be large enough to avoid contamination by the boundary forcing during a short experiment, and is well adapted for forecast experiments. Domain B is small enough to allow high resolution experiments, and to be free of large-scale errors due to imposing analysed values on its boundaries. The verification has been done essentially on Domain B.

A 'standard' proposal for the terrain height and roughness at 10 km resolution on Domain B was prepared by the organizing group (CNRM). This has been computed from higher resolution data, using an envelope-type formulation; precisely the average of the raw orography on the grid box plus one times the r.m.s. deviation of the subgrid-scale orography. For the roughness, a heuristic formulation of this same r.m.s. deviation, divided by a factor of 80 was used.

The initial and boundary data distributed for the second COMPARE exercise were provided from reanalyses of this case, performed by the European Centre for Medium-range Weather Forecasts (ECMWF), at resolution T213 and 31 levels. They cover the time period from 0000 UTC, 14 October to 0000 UTC, 16 October 1990, with 6 hour time intervals.

The analyses were performed on the 31 model levels, but for the convenience of participants, they have been reinterpolated to the same 44 pressure levels already used in the first COMPARE exercise: every 25 hPa from 1050 hPa to 100 hPa, plus the 70, 50, 30, 20, and 10 hPa levels. The fields include horizontal wind components (u, v), temperature (T), specific humidity (q), the surface pressure, and the consistent height of the orography in the ECMWF model. Various geophysical fields were also supplied.

All the proposed experiments start at 0000 UTC, 15 October and last for 18 hours. Many observations are available for verification between 0600 UTC and 1200 UTC, 15 October, and surface observations are still available until 1800 UTC. Remember that the peak intensity of the lee-wave and drag occurs at 0900 UTC, but the lee vortices occur at 1200 UTC and later.

- Experiment 1: This experiment is run on Domain A, with a resolution as close as possible to 50 km. The initial values are provided by the 0000 UTC, 15 October analysis, and the subsequent analyses are used to apply a larger scale forcing at the boundaries of Domain A. This is a basic 'forecast' experiment, designed as a reference to assess the benefits of increased resolution.
- Experiment 2: Domain A, but resolution close to 25 km. This is also a 'forecast' experiment. At this resolution, the orographic details of the area of interest are much better resolved, and some aspects of the regional wind systems appear, as well as improvement in the resolved pressure drag and mountain wave system.
- Experiment 3: This experiment is run on Domain B with a resolution close to 10 km, and driven by the results of Exp. 2. It is a 'forecast' experiment, because the results are not influenced by the analyses (except for the initial state). Further improvement of the surface wind and pressure field forecast was, of course, expected from Exp. 2 to Exp. 3.
- Experiment 4: This experiment is run on Domain B with the same resolution as Exp. 3, but driven directly by the analyses on the boundaries of Domain B: It is therefore (hopefully) free of large-scale errors. It should supply the best results, however this is clearly not a forecast, but a 'dynamical adaptation' experiment.
- Experiment 5: Same as Exp. 4, except that it uses the 'reference' 10 km resolution terrain height and roughness distributed to the participants (for experiments 1 to 4, the usual specification of orography and roughness, varying from one model to the other, is used).

In the present paper, we will report only the results of Exps. 3, 4 and 5, because they are the core of the intercomparison. Experiments 1 and 2 were run by most participants, and gave generally similar results. We should also mention that some participants reported on interesting additional experiments, especially lee-wave resolving simulations using non-hydrostatic models.

TABLE 1. LIST OF THE PARTICIPATING MODELS IN EACH EXPERIMENT

Institute	Model name	Non-hydrostatic	Experiments
JMA	JSM		3 5
FISBAT	BOLAM		3 4 5
CSIRO	DARLAM		3 5
CNRM	ALADIN		3 4
RPN	MC2	X	3 4 5
DWD	DM		3 4
UKMO	UKMO		3 4 5
NCEP	EMC		3 4 5
RPN	EFR		3 5
JMA	NHA	X	3 4
RER-SMR	LAMBO		3 4 5
INM	HIRLAM		3 4 5
CNRM and LA	MESONH	X	4
USNAVY	COAMPS	X	3 4 5
NCEP	RSM		3 4 5

(*c*) *The participants*

The participating institutions and models are listed in Table 1 and comprise:

- the JMA (Japan Meteorological Agency) Japan Spectral Model (JSM; Segami *et al.* 1989) and the MRI (Meteorological Research Institute) Non-Hydrostatic and Anelastic model (NHA; Ikawa and Saito 1991, Saito 1994)
- the FISBAT Institute BOlogna Limited Area Model (BOLAM; Buzzi *et al.* 1994)
- the CSIRO (Commonwealth Scientific and Industrial Research Organisation) model DARLAM (Division of Atmospheric Research Limited Area Model) (McGregor 1993, McGregor and Walsh 1994)
- the CNRM model ALADIN (Aire Limitée Adaption Dynamique dévelopment InterNational) (Bubnová *et al.* 1995) and the CNRM and LA (Laboratoire d'Aérologie) MESOscale and Non-Hydrostatic model (MESO-NH; Lafore *et al.* 1998)
- the RPN (Recherche en Prévision Numérique) Regional Finite Element model (EFR; Benoit *et al.* 1989; Mailhot *et al.* 1997) and the non-hydrostatic Mesoscale Compressible Community model (MC2; Benoit *et al.* 1997)
- the DWD (Deutscher WetterDienst Deutschland) Model, nested into the Europa-Model, (DM; Majewski 1997)
- the UKMO (United Kingdom Meteorological Office) Unified Model (Cullen and Davies 1991)
- the NCEP (National Centers for Environmental Prediction) 'ETA' model (EMC; Black 1994; Janjic 1994) and Regional Spectral Model (RSM; Juang and Kanamitsu 1994; Hong and Pan 1996)
- the RER-SMR (Regione Emilia-Romagna) LAMBO model (Limited Area Model BOlogna) (Paccagnella *et al.* 1992)
- the INM (Instituto Nacional de Meteorologia) HIgh Resolution Limited Area Model (HIRLAM; Källén 1996)
- the US-NAVY Coupled Ocean Atmosphere Mesoscale Prediction System model COAMPS; Hodur 1997)

(*d*) *Methods for data processing*

All results presented in this paper were elaborated at CNRM from the model outputs of the various participants. The available data for each model were: 2D fields of the model's surface geopotential; land/sea mask; surface pressure and surface temperature;

3D fields of u, v, T, q, Φ (geopotential); w (vertical velocity, diagnosed for hydrostatic models, and forecast for non-hydrostatic models); turbulent kinetic energy if available. The results are at 00 UTC, 03 UTC, 06 UTC, 09 UTC, 12 UTC, 15 UTC, 18 UTC, 15 October.

The basic principle was to reconstitute parameters directly comparable to the observational data, in order to conduct a direct validation using observations. To ensure an equal treatment of all participants, model fields were interpolated onto a common three-dimensional grid, the latter being used for the score computation. The routines used for the interpolation were those used for the evaluation of the CNRM operational model performances. However, as model topographies were different from each other, a specific vertical interpolation was developed. In this computation the planetary boundary layer (PBL) is stretched so that ground variables remain near the ground, whereas for variables at the top of the PBL the altitudes remain the same. During this interpolation the momentum and the relative humidity, as well as the distance between the potential temperature and a reference profile, are conserved.

For all participants the model results have been interpolated to the exact location of the observation using the 'observation guess' part of the data assimilation routine procedure of CNRM. Synthetic parameters, such as the surface pressure drag have also been computed and compared to the observations.

For the interpretation of the results, we will focus on four key characteristics of orographic flows among those mentioned in section 2(a): the local winds, the wake vortices, the shape of the mountain wave, and the pressure drag. To that aim we have split the available observations into various geographic areas shown in Fig. 4. These areas delimit the pertinent ground stations for each aspect of the flow. The area called 'Wake', is devoted to the vortex study and surrounds the zone of the return current of the vortex pair appearing in the observations. In the same area, at Lannemezan, there is a sodar which gives a description of the vortex structure between ground and 350 m. The area called 'Autan' corresponds to the location of the so-called local wind. A sodar in the same area gives additional information on this wind. The area 'Bochorno' goes with the Bochorno wind which blows into the Ebro valley where there is also a sodar. And finally the 'Adour' area goes with the river of that name. The 'Adour' zone, as it will be seen later is fed by air which crosses the mountain. Between 10 and 25 ground stations are located in each of these sub-domains. Along the line B1B4 three airplanes flew along 10 different legs, and gave a good description of the hydrostatic wave between 615 and 197 hPa. Also along this line, 14 microbarographs have allowed a very reliable calculation of the pressure drag.

All participating models have been evaluated using a point-to-point validation. Scores have been calculated for the aircraft and sodar observations for all domains. The scores we use are the root mean square error (RMS) and the bias. They are defined as follows:

$$RMS^2 = b^2 + \sigma^2$$

with the bias $b = \frac{1}{N}\sum_i^N Forecast_i - Observation_i$, and the square of the standard deviation of error $\sigma^2 = \frac{1}{N}\sum_i^N ((Forecast_i - Observation_i) - b)^2$. N is the total number of observations and RMS is a measure at the total error. In the case of missing observations, the RMS and bias are set to zero.

(e) *Problems encountered*

Any intercomparison exercise has its share of technical problems and unfortunately one error was discovered too late for correction. When preparing the GRIB files for

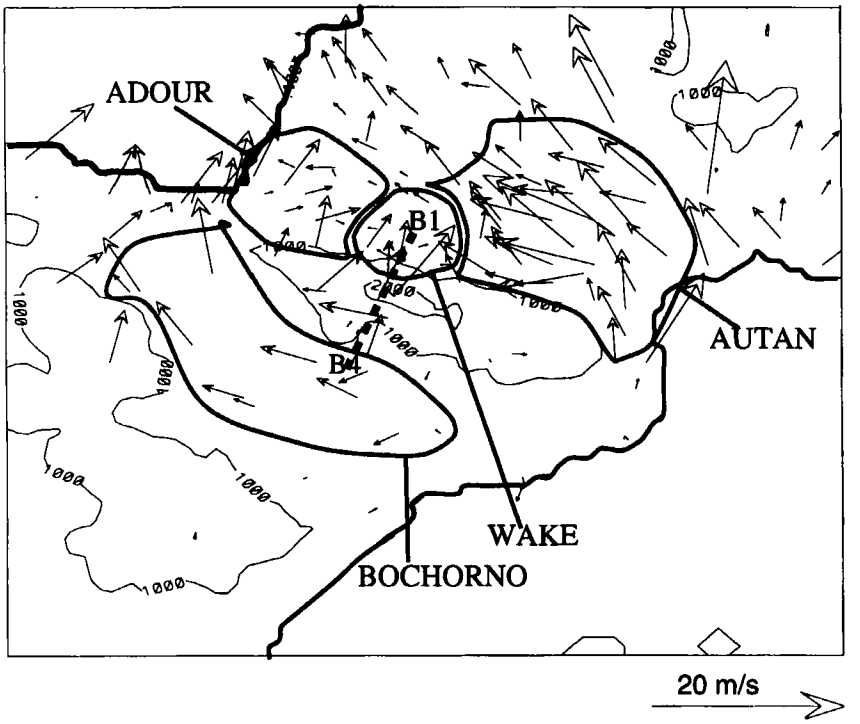

Figure 4. Areas for the scores computation; vectors represent observed surface winds (see text).

data distribution, a confusion was made between the nominal pressure values of the full levels and half levels of the interpolation grid. As a consequence, the data distributed had an average pressure error of 12.5 hPa, i.e. approximately 100 m in the lower atmosphere. It is difficult to estimate the full consequences of this error, but several arguments suggest optimism. The feedback of the temperature error on the dynamics of the waves can be estimated from the error in the Brunt–Vaisala frequency. The implied error in troposphere depth is about 100 m, which corresponds to a relative error of 1%, therefore the Brunt–Vaisala frequency, which varies as the square root of the potential temperature gradient, will have a 0.5% relative error. On these grounds, we estimated that the dynamical feedback of the above-mentioned vertical interpolation error is negligible, and proceeded to analyse the results.

3. Results of Experiment 3

Experiment 3 had the largest number of participants (14). The description of its results will thus take the major part of this paper. The discussion will be presented in such a way as to illustrate the main characteristics of the orographic flows discussed above.

(*a*) *Local winds*

At low level, the flow which impinges upon the Pyrénées splits into two branches: the eastern one goes around the mountain forming the Autan wind which is further re-accelerated by the narrowing of the valley between the Pyrénées and the Massif Central;

the western one is channelled by the Ebro valley and forms the Bochorno wind (see Fig. 4). Figure 5 displays the time evolution of the RMS of the wind intensity for the two corresponding areas. These results should be considered relevant only after 03 UTC, since the experiment begins at 00 UTC, and three hours are needed for the models to adapt to initial conditions (e.g. the behaviour of the LAMBO and ALADIN model for the Autan wind). In addition the Autan area becomes difficult to interpret after 12 UTC, because of the lee vortices development. Taking into account the above restrictions, one can observe that the value of RMS is stable with time for the Autan, around 3.5 m s^{-1}, the error is more variable for the Bochorno, but it remains less than or equal to the Autan value. Figure 6 shows the bias of the wind speed for the same two areas. A negative bias means that the simulated wind is weaker than the observed one. One can notice that for both areas the bias is negative for all models except the EMC, and also LAMBO for the Autan (yet, their RMS is as large as for other models). Forecasters for the Autan region confirm that predicted local winds are very often too weak. All models have a negative bias for the Autan wind direction, (Fig. 7), which signifies that the forecast winds have too big a northerly component. It is worth noting that the exception is again the LAMBO model. Since this regional wind rotates around the edge of the mountain, its curvature radius is a function of its speed and this may explain the correlation between the wind strength and wind direction. In contrast, for the Bochorno wind, the bias is around zero, which was expected because this local wind is more channelled into a deeper valley.

To understand this general behaviour of the models, it is useful to look at scores in the Adour zone (Fig. 8). This zone is downwind of the mountain and Fig. 9 shows how it is fed by the air flowing above and across the Pyrénées. It is also the place where the onset of the Foehn was first observed. In Fig. 8 it is clear that most models overpredict the wind intensity, and this means that the predicted part which goes above the mountain is stronger than the observed one. This behaviour highlights the local wind scores; if local winds are too weak, it is because the part of the flow that goes above the mountain is too large compared with the part going around it. The blocking appears to be insufficient. Now let us go back to the exception we have found; the EMC which has too strong Autan and Bochorno and the LAMBO which also has too strong an Autan wind. One should recall that these models are derived from the ETA-model (Mesinger *et. al.* 1988). These two models can produce stronger local winds than the others, but it does not seem to be the result of a better representation of blocking since they follow the other models in Fig. 8. The choice of the vertical coordinate cannot be an explanation either because the LAMBO has chosen a sigma coordinate for this simulation.

The comparison with the sodar measurements (not shown) shows that the error becomes much larger a few hundred metres above ground (up to -8 m s^{-1} for the bias!).

(*b*) *Lee vortices*

Figure 9 represents the time evolution of the observed surface wind, in particular the appearance and disappearance of the pair of lee vortices. At 12 UTC some northern winds (i.e. reversed winds) appear downwind near the centre of the Pyrénées which is the return current of a pair of counter-rotative lee vortices. At their maximum, at 15 UTC, their width is about one hundred kilometres. At 18 UTC, in the centre of the mountains, the wind has turned from north to south; to the west of the range some smaller vorticity is found. Between 15 and 18 UTC the lee vortices shrink and move westward. It is difficult to define a reliable score for a vortex; for very weak winds (<3 m s^{-1}), wind direction has no sense and is not computed, and if a model well reproduces the shape of the lee vortices but shifted eastward (for example) the direction will change dramatically by

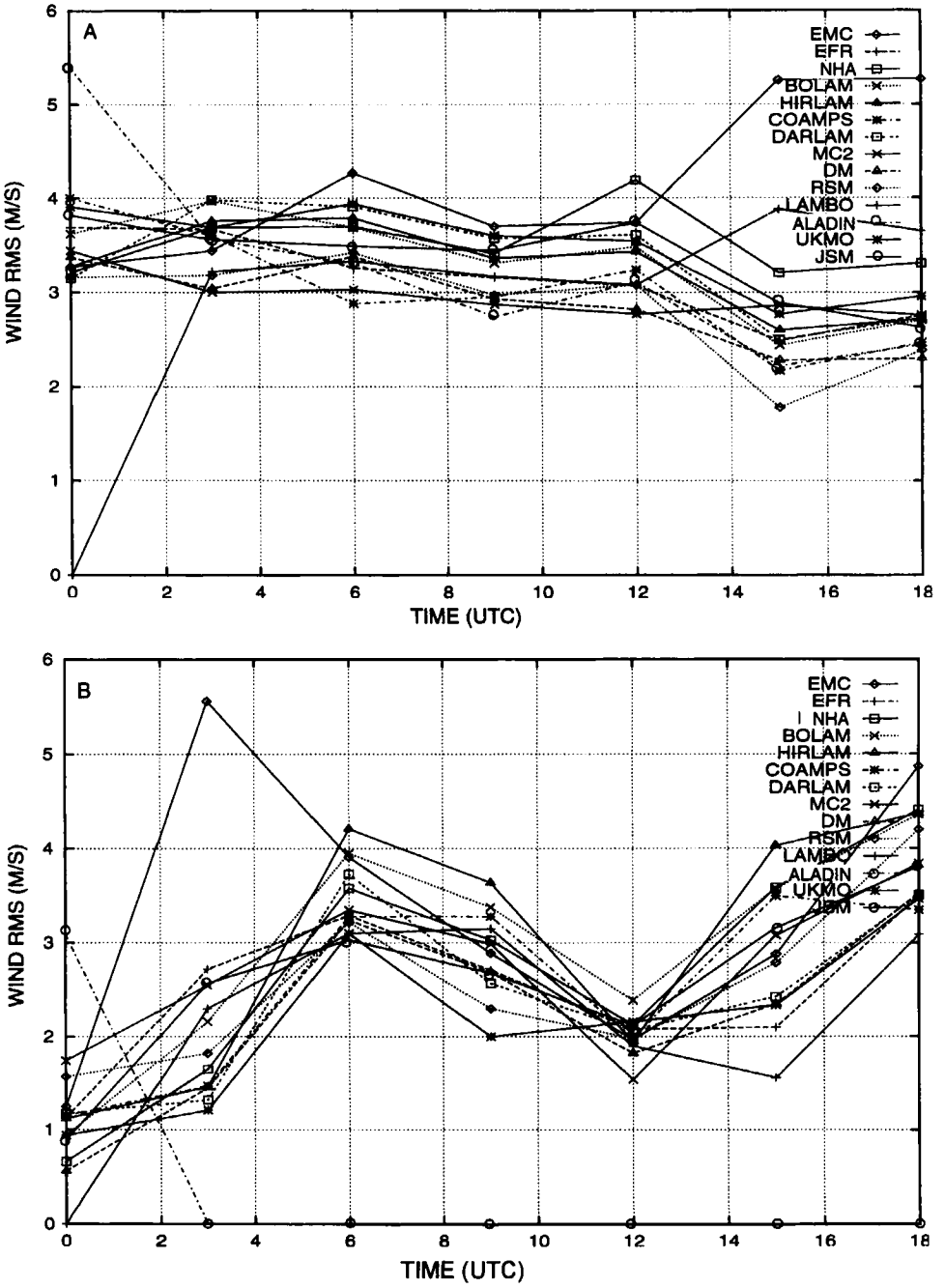

Figure 5. Time evolution of the RMS against observations of wind intensity, for Exp. 3. (A) for the Autan area. (B) for the Bochorno area.

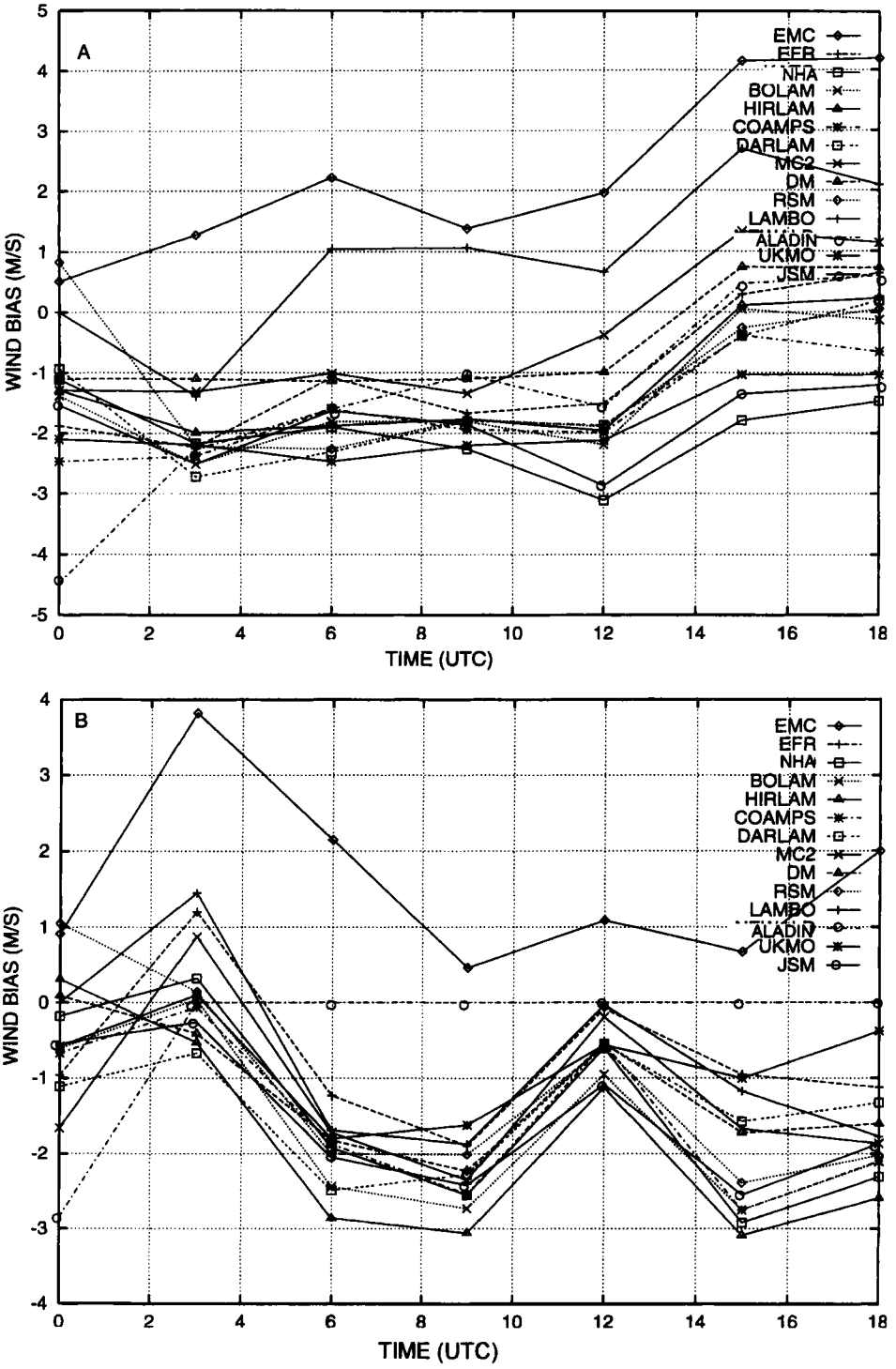

Figure 6. Time evolution of the bias against observations of wind intensity, for Exp. 3. (A) for the Autan area. (B) for the Bochorno area.

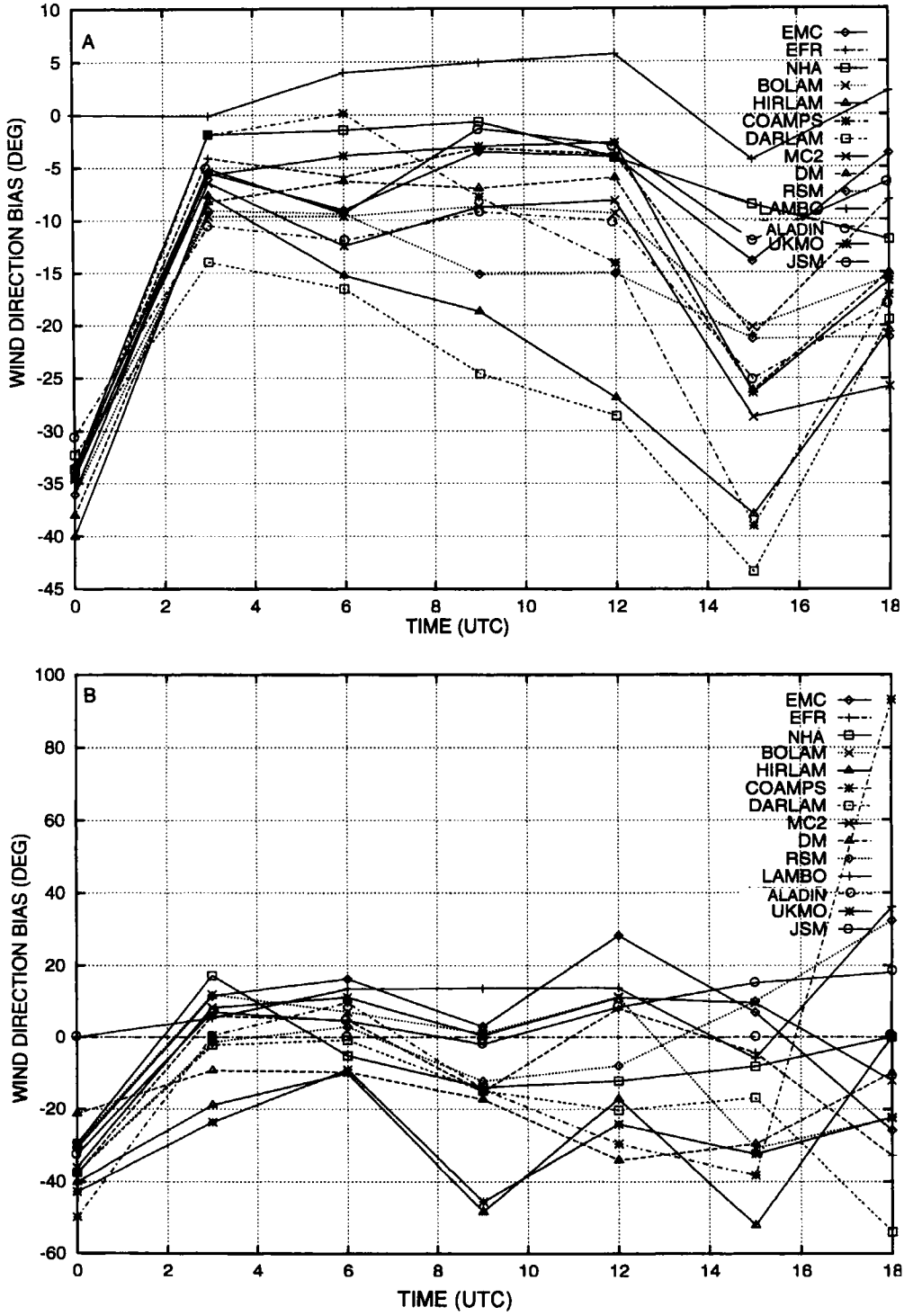

Figure 7. Time evolution of the bias against observations of wind direction, for Exp. 3. (A) for the Autan area. (B) for the Bochorno area.

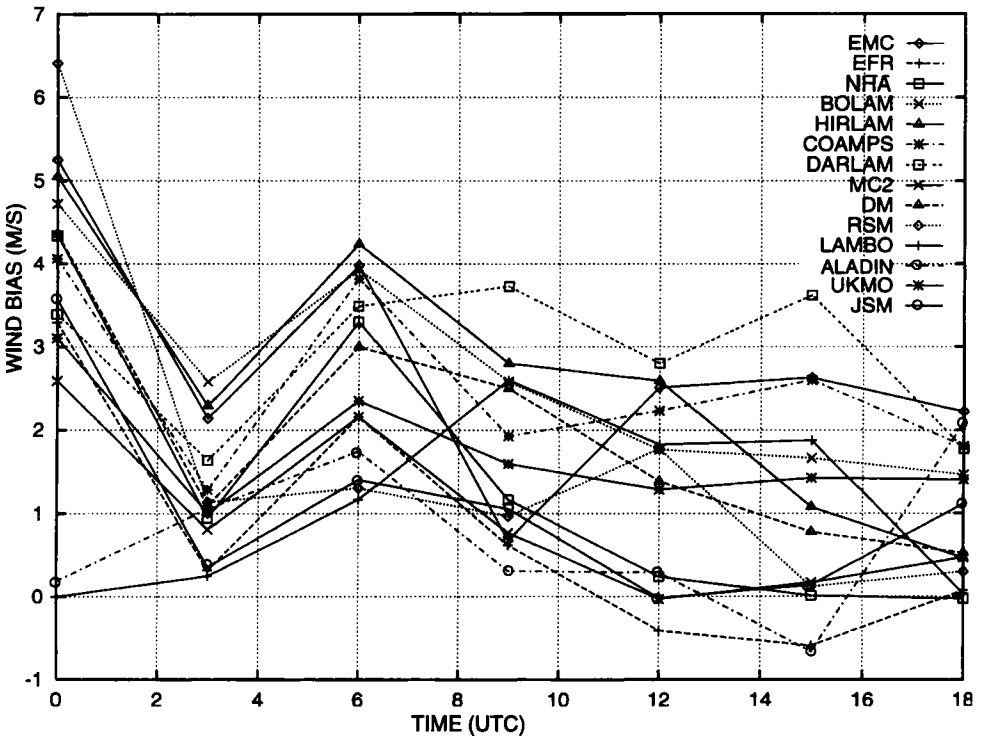

Figure 8. Time evolution of the bias against observations of wind intensity for the Adour area for Exp. 3.

about 180 degrees. The scores should be complemented by some direct visualization of the surface wind field. Figure 10 presents the bias in wind direction for the 'Wake' area. This area surrounds the reversed current of the lee eddies, at 12 and 15 UTC. A bias greater (smaller) than 90 (−90) degrees means that there is no reversal of the flow, and thus no lee vortices occurred at this place, (when the direction is not computed the bias is set to 0). On this picture one can see that the error growth is coincident with the vortices development. Figure 11 shows a comparison with the Lannemezan sodar results: the first column corresponds to the observations at 15 UTC between ground and 350 metres, the other columns correspond to the simulated wind, at the same location and same time, for each participating model. The observed north wind is the signature of the return current of the two counter-rotative eddies, and only two models out of fourteen (RSM and ALADIN) could reproduce the observed reversed flow. Looking at the surface wind fields of the models, it appears that half the models have no vortex at all at 15 UTC; for the others the vortices sometimes appear too early, are not located at the right place and are in general over developed at 18 UTC. The forecast of lee vortices seems therefore to be a difficult task for mesoscale models.

(*c*) *Mountain wave*

The wind and potential temperature fields of a mountain wave system will typically show a wavy pattern, when plotted along a pressure leg. Between 06 and 09 UTC, three planes took measurements along 10 different pressure legs. Scores have been calculated for each leg for potential temperature and the wind component perpendicular to the ridge. In addition, to have a more global view of the results, two global scores (for wind

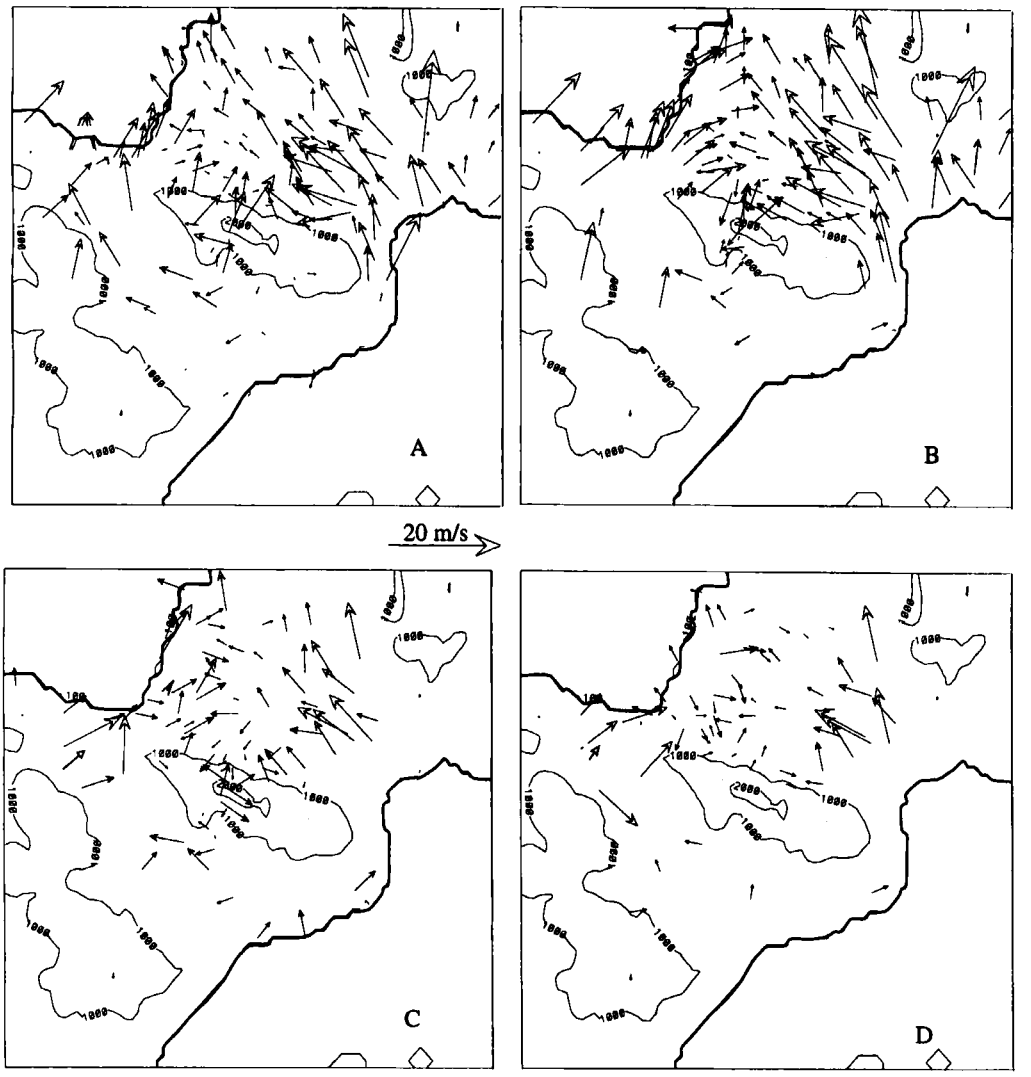

Figure 9. Time evolution of the observed wind field at the ground. (A) 09 UTC (B) 12 UTC (C) 15 UTC (D) 18 UTC.

and temperature) have been evaluated by combining the 10 scores. Figure 12 shows the RMS scores against pressure. The RMS for the cross-mountain wind component, is around 5 m s^{-1} except at about 350 hPa where most models show a bigger error. Looking at the wind field it seems that the strong error at this altitude is mainly linked to a bias against the upwind conditions. It may be caused by a problem with the upwind initial conditions, or with the nesting in Exp. 2. On the same figure, the RMS scores against potential temperature are shown. The values are quite good; the error is around 2 K at low level and increases with altitude up to 6 K at the tropopause. However, there is no error peak at 350 hPa as occurs for wind. Looking at each model's winds and temperatures along a pressure leg allows us to better explain these scores. Figure 13 shows the ARAT 545 hPa leg for cross-mountain wind and temperature. The observed and simulated variables are presented together along the flight track which is about 200

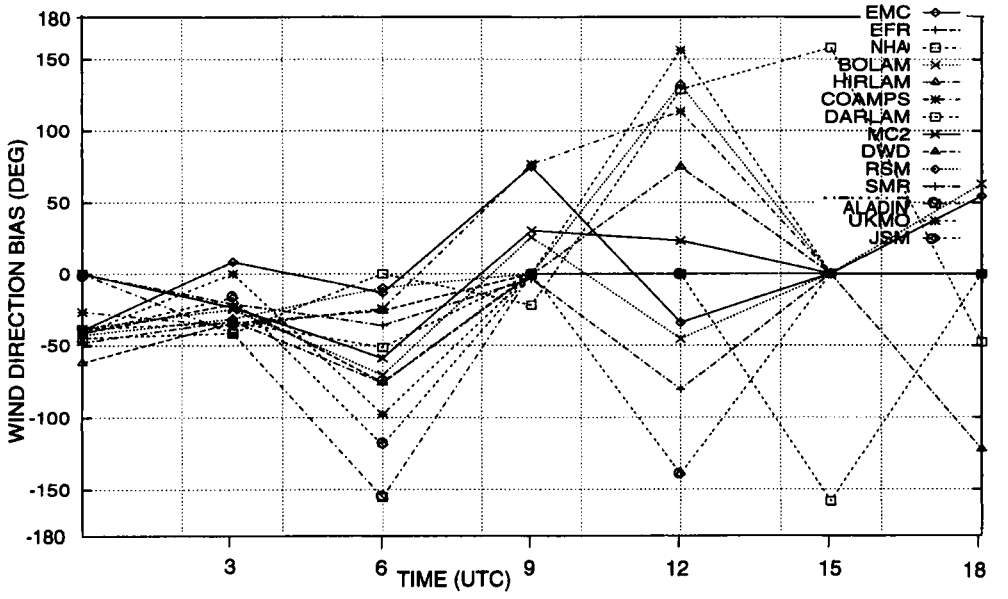

Figure 10. Time evolution of the bias against observations of wind direction for the Wake area for Exp. 3.

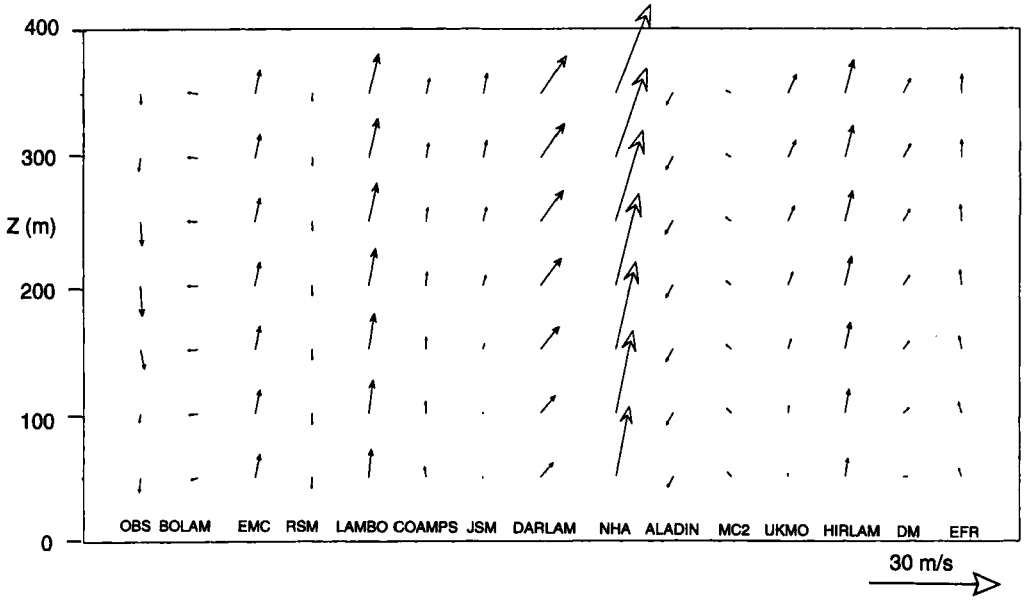

Figure 11. Comparison between model results and sodar measurements for the horizontal wind on the first 350 m above Lannemezan at 15 UTC, for Exp. 3.

kilometres long. On the wind figure, all models have stronger winds than those observed on the upwind edge. This bias explains a part of the total error, but the major part of the RMS comes from the over-estimation of the wave amplitude by the majority of the models. The temperature picture also shows the over-estimation of the simulated waves, but it does not seem to reveal any bias at the upwind edge.

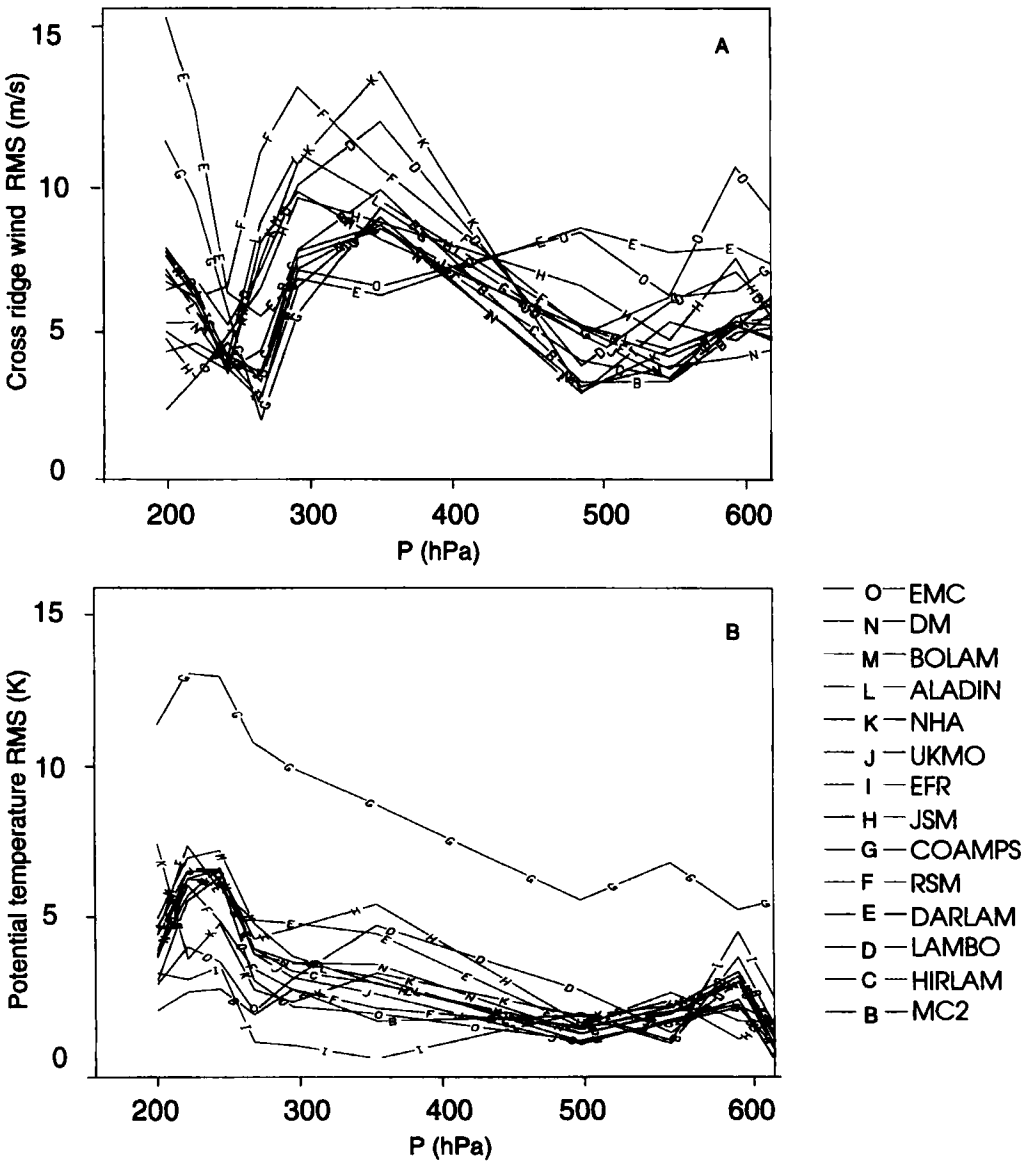

Figure 12. RMS against aircraft measurements versus pressure altitude, for Exp. 3. (A) for the cross-ridge component of the wind; (B) for the potential temperature.

The fact that the wave amplitude is in general over-estimated by the models seems consistent with the fact that these models are not creating enough blocking to have the right local-wind amplitude. There is not enough air diverted around the Pyrénées, and thus there is too big a part of the atmosphere crossing the mountain and so participating in the mountain wave mechanism. The mountain wave becomes too strong although the height of the topography, which is exciting this wave, is smaller than the real one.

At the tropopause level, the aircraft measurements exhibit a secondary wave at about 80 km downstream of the main wave. The existence of this secondary wave is attributed

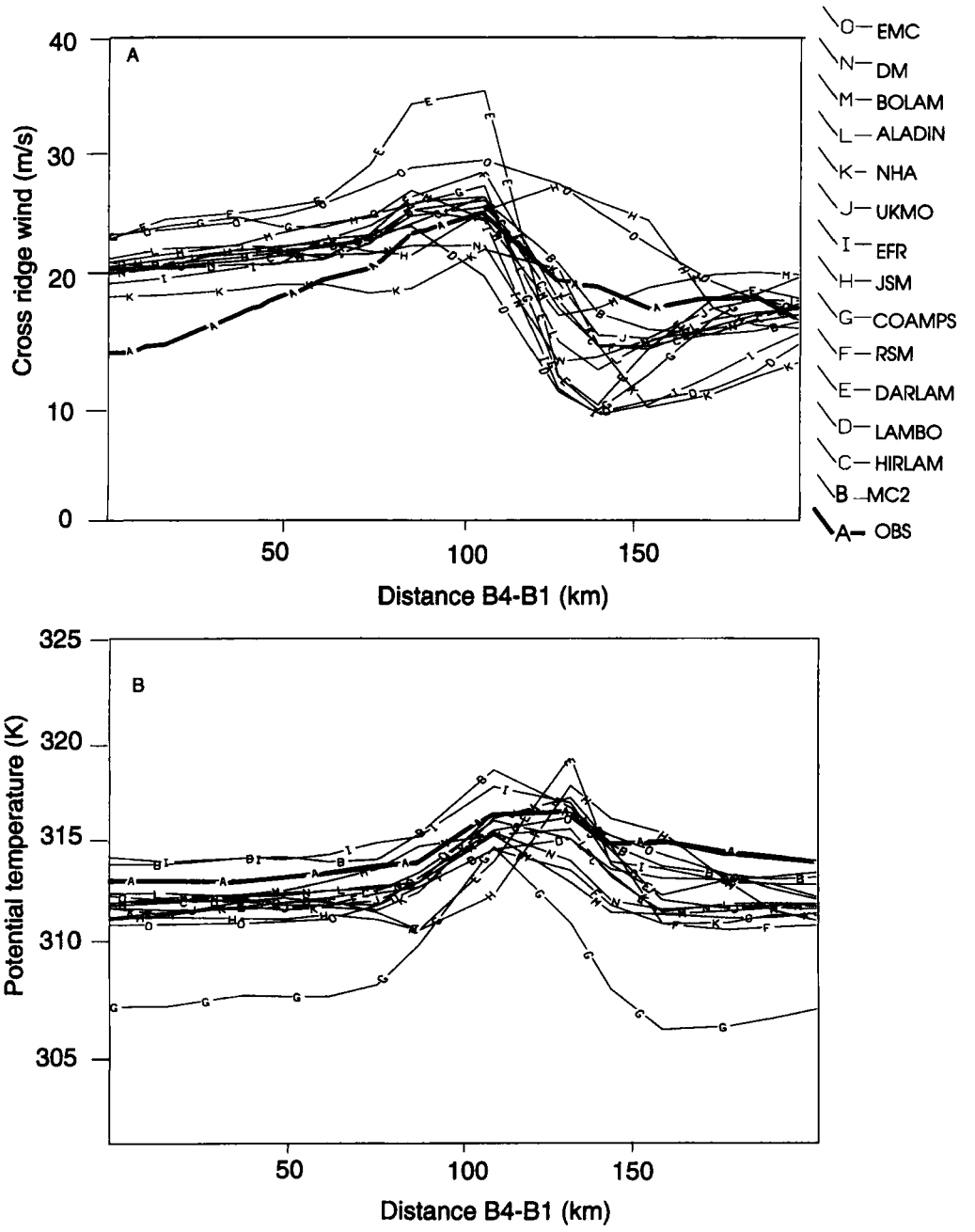

Figure 13. Comparison between model results and aircraft measurements (thick line) along the 545 hPa leg, for Exp. 3. (A) for the cross-ridge component of the wine; (B) for the potential temperature.

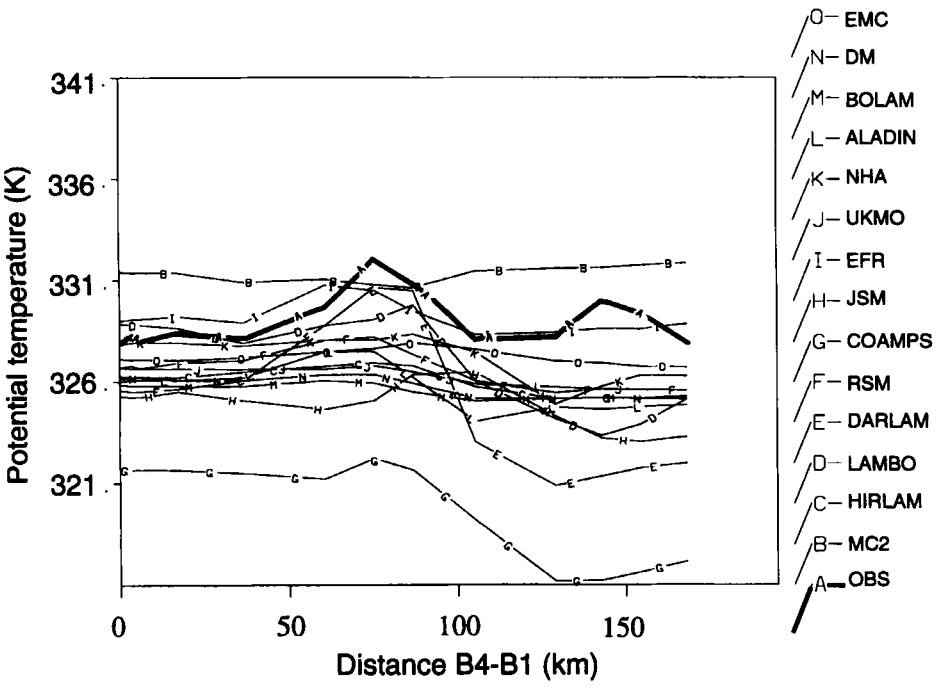

Figure 14. Observed (thick line) and simulated potential temperature along the 288 hPa leg, for Exp. 3.

to non-hydrostatic effects. Figure 14 presents the 288 hPa FALCON leg; one can notice that no models have been able to reproduce this feature, even the non-hydrostatic ones.

The global scores, taking into account all the legs, are presented in Table 2; they allow us to identify which kind of model is more efficient for mountain wave representation. For potential temperature the global RMS lies between 2 and 3.25 K (except for one model), which is quite a good score, and the model results are quite close to each other. On the other hand, the global score for the cross-ridge component of the wind goes from 5 to 8 metres per second. In Table 2, the various models are classified according to their scores using potential temperature and wind along the cross-section followed by the planes. To this table have been added the main characteristics of the different models in connection with the relief treatment. It appears that the model scores are strongly correlated with the technique for topography representation, in particular as regards the roughness parametrization. The models which are the most successful in simulating the IOP3 mountain wave are generally those which use a low orography (or mean orography) together with an effective roughness length (of the order of 10 m) representing the subgrid scale variation of topography. Among the models using a large roughness, those with the largest have the smallest wave amplitude (but still too strong compared to the observations). Therefore the envelope orography does not seem to be an adequate parametrization to give the right wave field.

(*d*) *Pressure drag*

In the PYREX experiment, the drag was evaluated using 14 microbarographs along a cross-section of the Pyrénées (see Fig. 1). In the present project, the drag simulated by

TABLE 2. GLOBAL SCORES AGAINST THE AIRCRAFT MEASUREMENTS. MODELS ARE CLASSIFIED WITH RESPECT TO THEIR RMS IN POTENTIAL TEMPERATURE (FIRST COLUMN) AND WITH RESPECT TO THEIR RMS IN CROSS-RIDGE WIND (SIXTH COLUMN). THE CORRESPONDING MODEL CHARACTERISTICS CONCERNING THE OROGRAPHY TREATMENT ARE INDICATED.

rank theta	mod	Mean orography	envelope	Zoeff	rank V	mod	Mean orography	envelope	Zoeff
1	EFR	X		X	1	DM	X		X
2	MC2	X		X	2	UKMO	X		X
3	EMC	X			3	MC2	X		X
4	UKMO	X		X	4	EFR	X		X
5	ALADIN		X	X	5	HIRLAM	X		X
6	HIRLAM	X		X	6	BOLAM	X		X
7	RSM		X		7	ALADIN		X	X
8	DM	X		X	8	JSM		X	X
9	NHA		X		9	NHA		X	
10	BOLAM	X		X	10	RSM		X	
11	LAMBO	X			11	COAMPS	X		
12	DARLAM		X		12	LAMBO	X		
13	JSM		X	X	13	EMC	X		
14	COAMPS	X			14	DARLAM		X	

the models was computed using the same method as in Bessemoulin *et al.* 1993:

$$D = \frac{1}{L} \int_{Zdown}^{Zup} \Delta P(Z)\, dZ.$$

Where D is the drag in Pa, P the pressure (Pa), *Zup* the altitude of the ground station at the upper level, *Zdown* the altitude of the ground station at the lower level and L the length of the section. $\Delta P = Pupwind - Pdownwind$ at the same altitude Z. In each model the predicted drag has been evaluated using the simulated geopotential at the same location as the microbarographs. Figure 15 represents the time evolution of the pressure drag. The mountain drag is negative here because the IOP3 has a southern flow. The simulated pressure drag is generally stronger (in its absolute value) than the observed one, except for one model which stands out from the rest. Some models simulate a drag remarkably close to the experimental one, given the fact that the drag is a second-order variable and therefore difficult to reproduce. The shape of the observed drag curve is well simulated, e.g. the relative maximum in the curve at 09 UTC is reproduced by nearly all models. Since the pressure drag is generally seen as a measure of the wave amplitude, we would expect the drag value of the various models to be correlated with their ability to represent the wave field. But comparing Fig. 13 with Fig. 15, it surprisingly appears that some models can have a correct drag with too big a wave amplitude or can have too strong a drag with one of the best simulated waves. The absence of a correlation between wave and pressure drag scores can be explained in two ways. The lowest altitude where the planes have flown is about 4 km, and below this limit the wave structure is unknown but does participate in the momentum flux budget and hence to the drag. Moreover, the first microbarographs involved in the drag computation are in the lee vortices circulation; too bad a representation of the wake by the models (which is here often the case) could influence the drag. Benech *et al.* (1998) have pointed out that in the whole of the PYREX data the intensity of the local winds is correlated with the drag intensity. Comparing Fig. 5 with Fig. 15 shows that models with a weak error in wind intensity generally have a good drag, and that models with too weak a local wind intensity generally have too strong a drag (still coherent with the fact that there is generally not enough blocking).

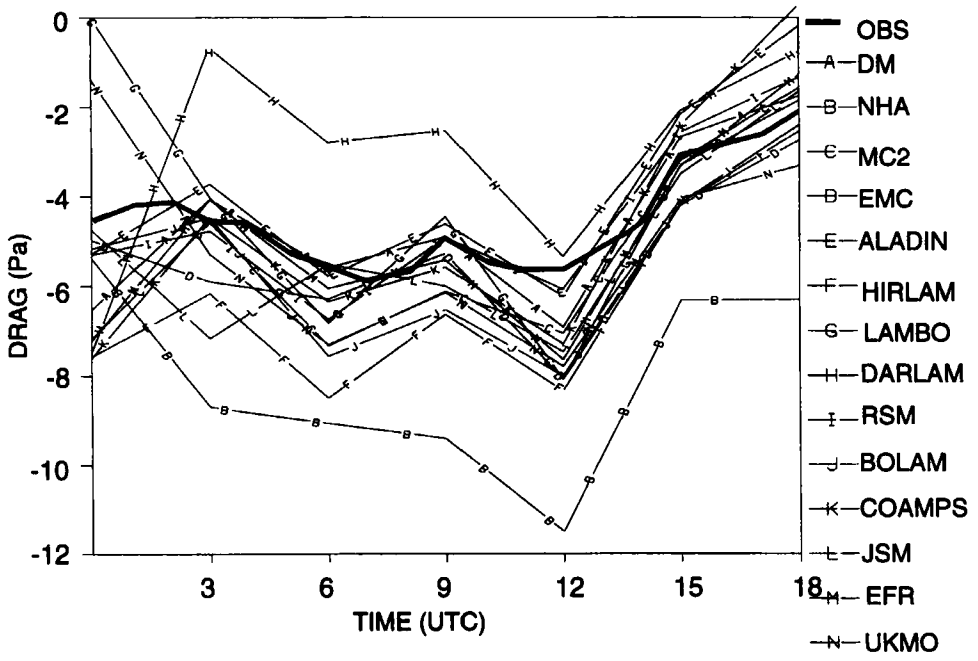

Figure 15. Time evolution of the observed (thick line) and simulated pressure drag for Exp. 3.

(*e*) *Discussion*

For Exp. 3, it appears that the main deficiency of the models is that they are not producing enough blocking, hence giving too weak local winds and too strong waves. Models using an effective roughness length together with a mean orography better simulate the mountain wave. The lee vortices seem to be the hardest flow feature to predict. Since the majority of the models have over-developed wake vortices at 18 UTC, and totally fail to describe the wake at 12 UTC and 15 UTC (where the vortices reach their maximum size), it suggests that the wrong forecasts could be due to a delay in the creation mechanism of the lee eddies. A second-order quantity like the drag has been quite well predicted, but we found little ability to represent the (observed) wave strength. This makes us wonder whether the drag is relatively well predicted for sensible reasons or not. Anyway, the correlation we have found with the local wind intensity makes the drag a useful diagnostic quantity.

4. Results of Experiment 4

Experiment 4 should be considered as a dynamical adaptation rather than a forecast experiment, since the lateral boundary conditions are forced towards the analysis. Twelve models have performed this experiment of which eleven have also done Exp. 3. Between these two experiments the model configurations have not been changed, so the results of both experiments can be compared in such a way as to highlight the impact of the large scale forcing.

(*a*) *Local winds*

Figure 16 displays the RMS and the bias for the Autan wind intensity, and comparing this figure with Fig. 5 and Fig. 6 reveals that, for the majority of the models, there has

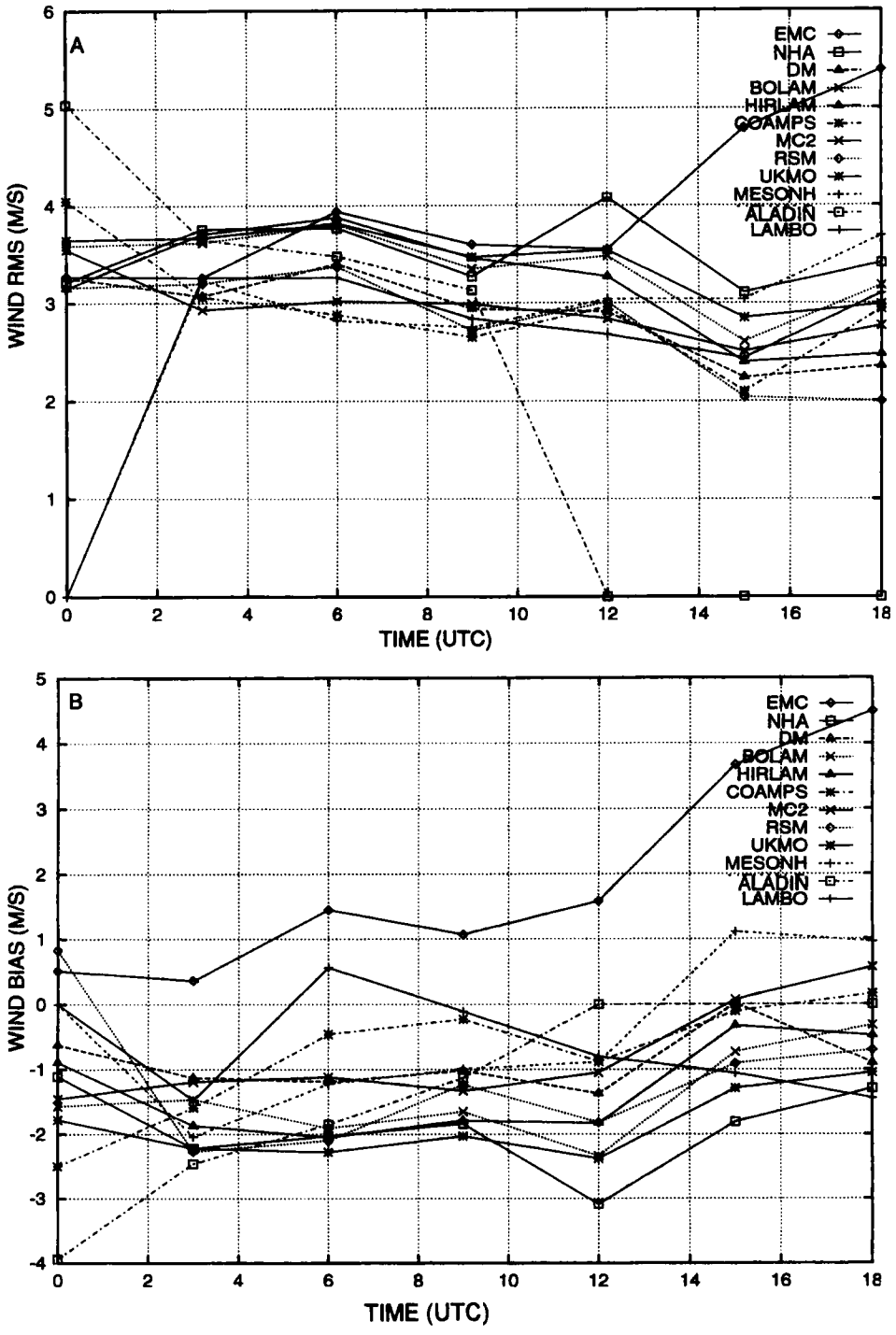

Figure 16. Time evolution of the scores against observations of wind intensity, for the Autan area in Exp. 4. (A) RMS; (B) bias.

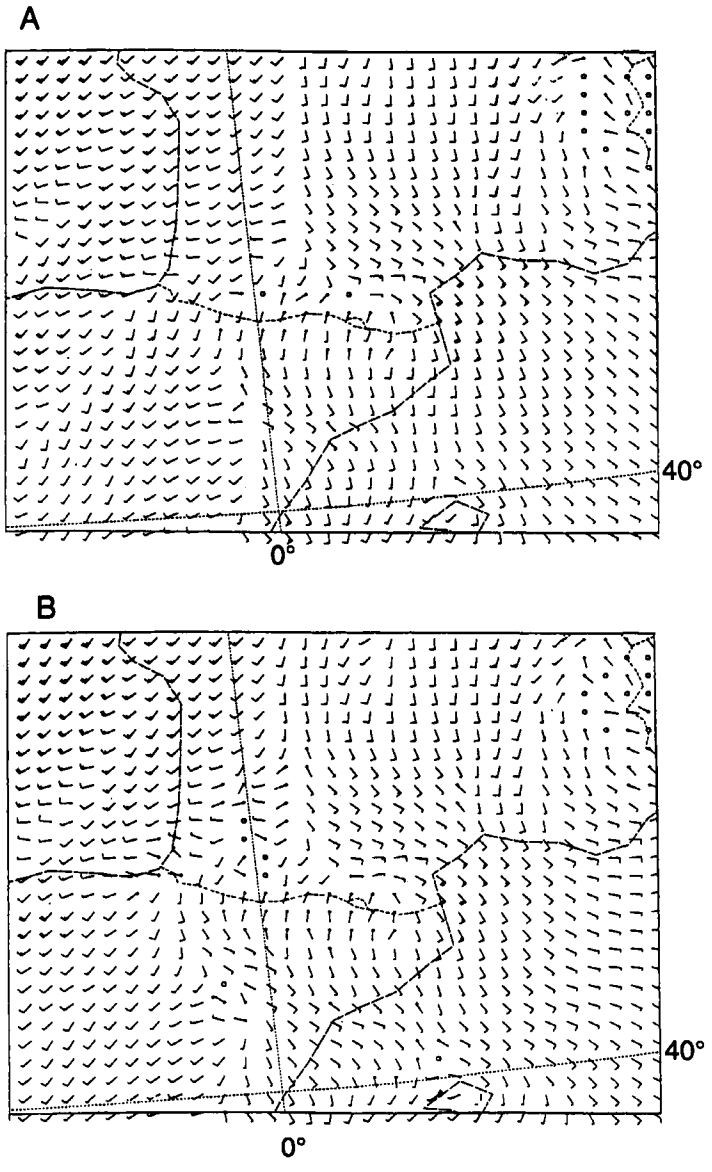

Figure 17. Ground wind field (wind barbs) at 15 UTC for the UKMO Unified Model. (A) Exp. 3; (B) Exp. 4.

been no improvement from Exps. 3 to 4. The scores keep very close to those obtained in Exp. 3. The same conclusion applies for the Bochorno (which could even be considered as slightly worse) and for the wind directions in the two areas. The correction of an *a priori* large-scale error does not lead to any improvement of the local winds, hence the error for local winds is related to the representation of orography.

(*b*) *Lee vortices*

On the contrary, the simulation of the wake gives different results from Exp. 3. Figure 17 shows an example of the ground wind field for the same model (UKMO) for Exp. 3 and Exp. 4. The wind intensity is modified in the wake, in Exp. 4 the

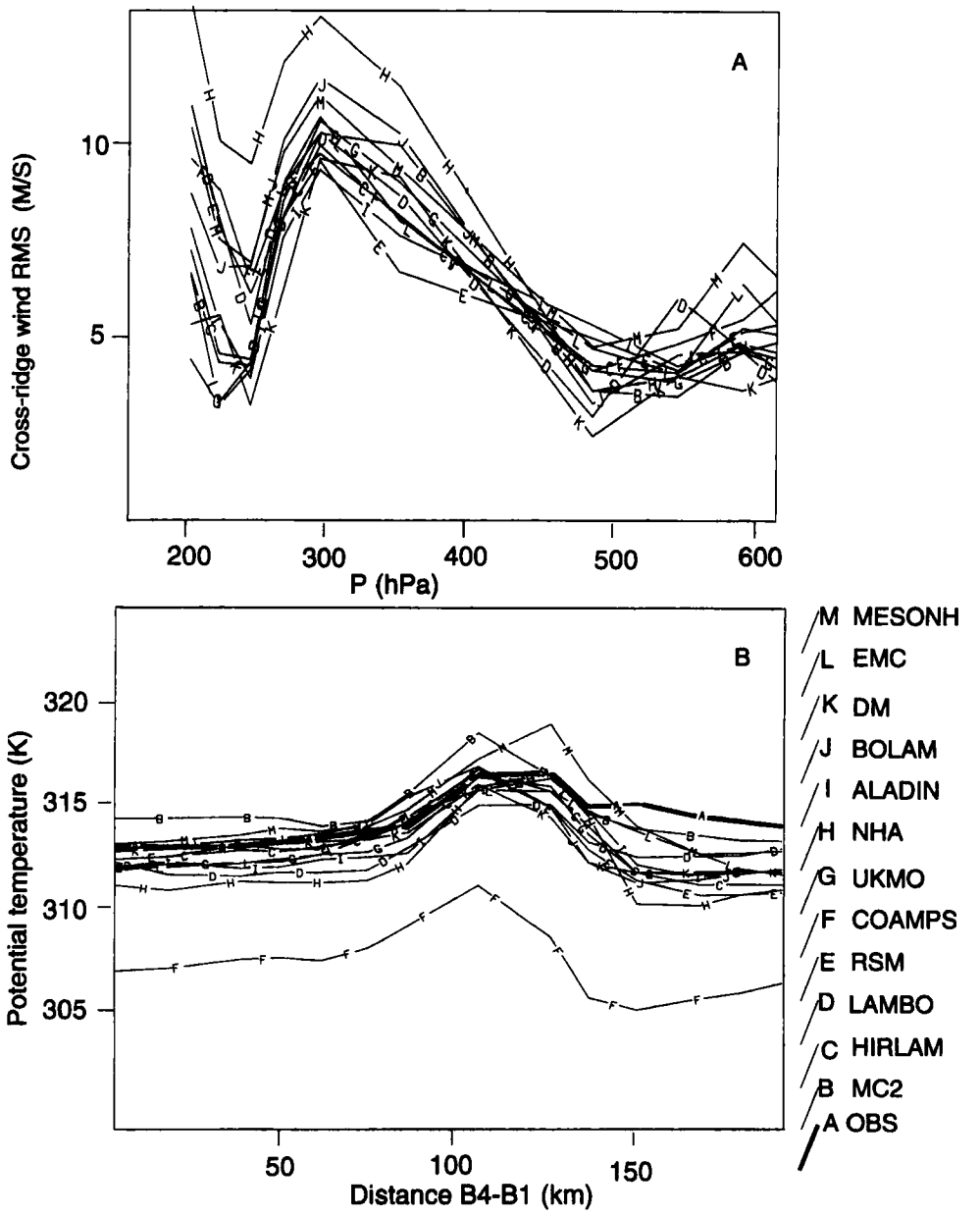

Figure 18. (A) RMS against observations of the cross-ridge component of the wind versus altitude, for Exp. 4. (B) Observed and simulated potential temperature along the 545 hPa leg, for Exp. 4.

wind is weaker around the Greenwich meridian whereas it is slightly stronger on the eastern side of the mountain (which is along the border). The wind direction is also different in Exp. 4 in the vicinity of the Greenwich meridian where there are more wind vectors whose direction is towards the south of the domain (i.e. a reversed wind). Similar considerations are valid for many models participating in Exp. 4, which means that there is a general trend to form vortices. Models which already have wake eddies in Exp. 3, now have them more strongly and more correctly located. In a global view the forecast

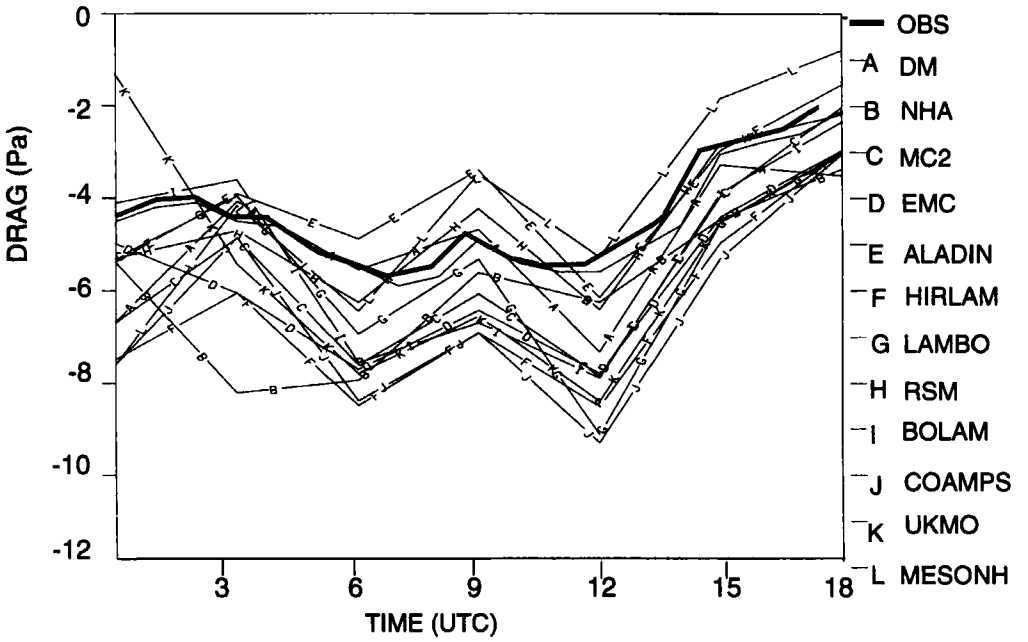

Figure 19. Time evolution of the observed (thick line) and simulated pressure drag for Exp. 4.

of the wake is still not a success, nevertheless a few models are now doing quite a good job in simulating correctly the lee vortices as they are at 15 UTC but all models fail in describing the evolution of the vortices between 15 and 18 UTC. Generally speaking the wake simulation has been improved by the improvement of the large-scale forcing; for example in Fig. 17 one can notice that, south of the Gascogne gulf (on the middle of the western boundary) the incoming flow can be very different between the two experiments and it might play a role in the wake circulation.

(*c*) *Mountain wave*

Figure 18A presents the vertical profile of the RMS against the plane measurements for the cross-ridge component of the wind. Comparing this figure to Fig. 12 (Exp. 3) (and Fig. 18B with Fig. 13B) shows that the range of values are the same, and the shape of the curves are very similar, but there is less dispersion in Exp. 4. From the first remark one can deduce that no major improvement is produced by the improvement of the large-scale forcing. On the other hand, the second remark indicates that some models which were too far removed from the mean behaviour are gathered nearer to the others by using a common large scale forcing. This indicates that a relatively small fraction of the total error is model dependent and related to *a priori* large-scale errors from Exp. 1 and Exp. 2, while the major part of the error is related to the orography representation. For the models which were going the wrong way without a correct large-scale forcing the forecast is improved, for the others the same causes of error are still present; a forcing with analysis has not corrected the upwind discrepancy between the observed plane wind and the whole of the simulated winds. The RMS profile still shows a peak of error around 300 hPa.

(*d*) *Pressure drag*

Figure 19 represents the time evolution of the observed and simulated pressure drag; comparing with Fig. 15 for Exp. 3 it appears, contrary to the previous result, that the different curves are not more grouped in Exp. 4 than in Exp. 3. This confirms the fact that there is no obvious link between the wave amplitude (between 615 and 197 hPa) and the pressure drag. Note, for instance, that the NHA model which is an outlier in Exp. 3, has significantly improved its drag in Exp. 4, whereas the simulation of the mountain wave by this model is not really improved in Exp. 4.

(*e*) *Discussion*

Experiment 4 indicates that there is an effect of the large-scale on small-scale features, such as the lee vortices, and the mountain wave. The introduction of a forcing by the analysis improves the lee vortices simulation, it also prevents the simulated waves from departing too much from the observation. The drag behaviour does not seem to be naturally linked to the one of the wave. Except from the wake, there is no general improvement from Exp. 3 to Exp. 4.

5. Results of Experiment 5

Eleven models participated in Exp. 5. Between Exps. 5 and 4 the experimental procedure remained the same, except that a reference topography and a reference roughness were prescribed. Eight models are common to Exps. 5 and 4, and for six of them, the topography has changed from a mean orography to an envelope orography, (the two others had it already). The maximum height of the mountain was then increased by about 500 m. Since in Exp. 4 all roughness parametrizations are the modellers' own choice and are very different from each other, its impact could not be isolated when comparing Exp. 5 results to those of Exp. 4; only the net effect of the envelope orography parametrization could be estimated.

(*a*) *Local winds*

The local wind RMS and bias for direction are, in a global view, unchanged compared to Exps. 4 and 3. The same feature is found again: the local winds are oriented too much towards the north. Figure 20 shows the Autan wind direction bias, which can be compared with Fig. 7. The bias against the Bochorno wind intensity could even be considered to be worse than in Exp. 3 (and 4) (see Fig. 6). The same result is found for the Autan wind intensity and the diagnosis of the error remains the same: the local winds are too weak. As in Exp. 4 (and 3) the EMC and LAMBO are exceptions, but it now appears that the reason for their particular behaviour has nothing to do with the choice in orography representation or in roughness parametrization. The envelope orography proves unable to enhance the local wind intensity. The sodar in the Autan zone, which gives a view of the Autan wind with altitude, indicates that the two models have progressed, but generally the scores remain the same.

The Adour region, whose flow is considered as fed by the air crossing the mountain, gives different results between Exp. 4 and Exp. 5 (Fig. 21). In Exp. 5 the bias is smaller than in Exp. 4 (of about 1 m s^{-1} in average) between 3 and 12 UTC. The bias, and so the RMS, have improved. The fact that the Adour bias is reduced indicates that there is less air crossing the mountain than in Exp. 4 simulations. Here the envelope orography seems to behave as expected since the blocking is enhanced. An explanation of these paradoxical results could be that the envelope orography parametrization smooths the

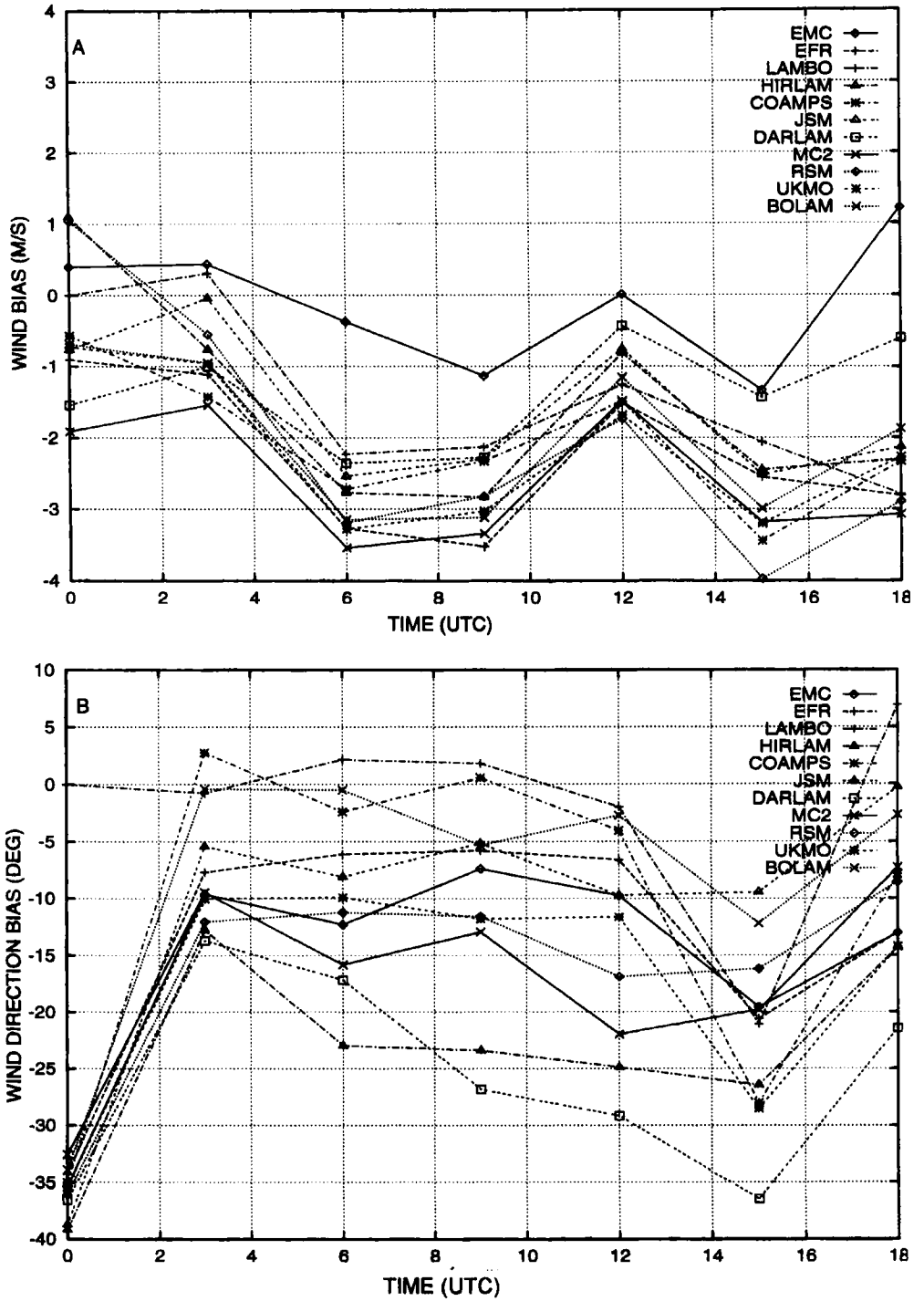

Figure 20. Exp. 5: Time evolution of the bias against observations of (A) wind intensity of the Bochorno; (B) wind direction of the Autan.

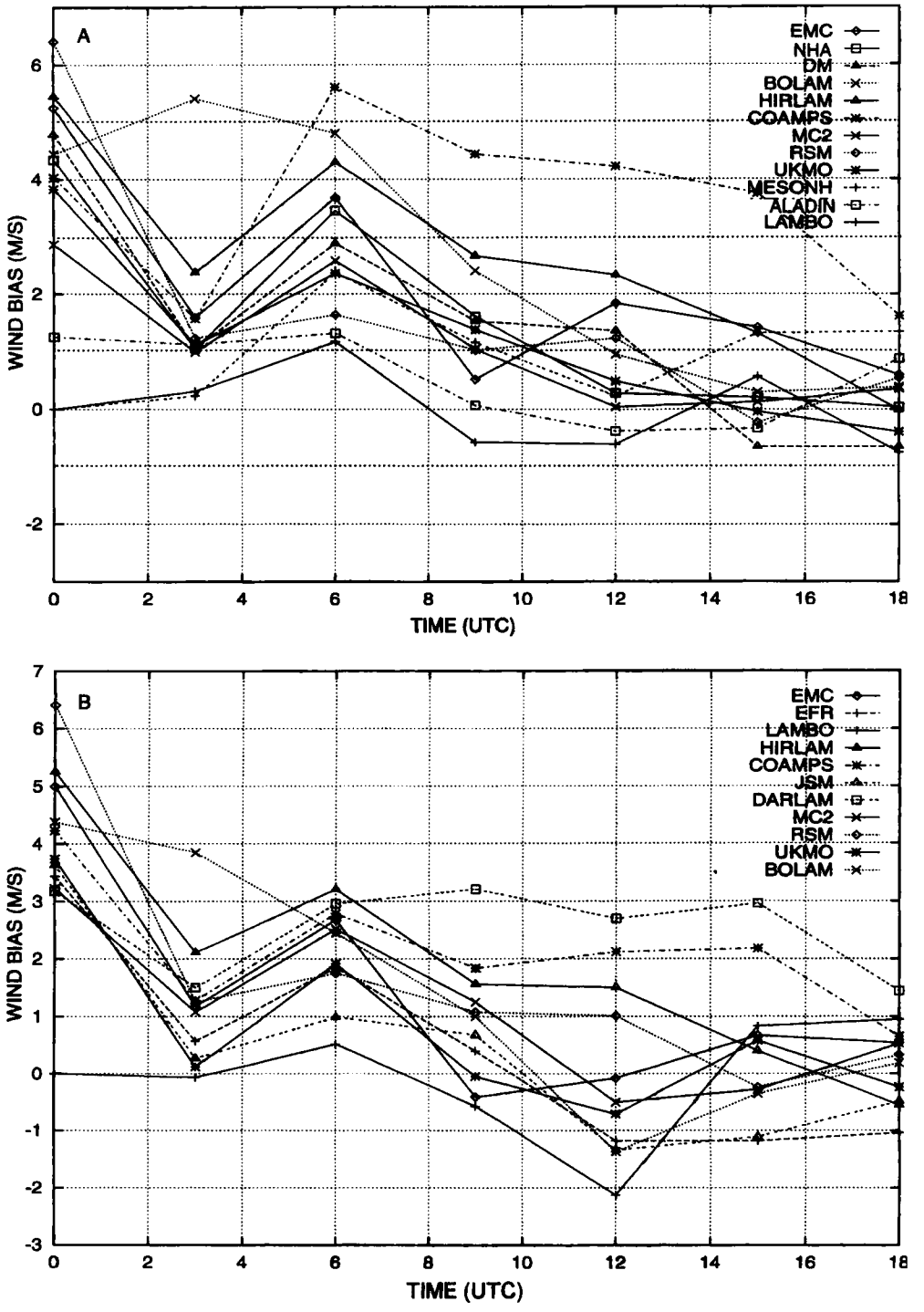

Figure 21. Time evolution of the bias against observations of wind intensity for the Adour area. (A) Exp. 4; (B) Exp. 5.

topography and 'fills' the bottom of the valleys, therefore the valley narrowing between the Pyrénées and the Massif Central is reduced, and the Ebro valley becomes less deep. The mechanism of acceleration of these winds, due to a Venturi-like effect, is less efficient as it results in a decrease of the surface wind which acts against the gain of wind intensity expected from a stronger blocking. The examination of the surface wind fields confirms that there is more blocking with the envelope. It also appears that generally the surface flow is stronger than in Exp. 4 when above the sea, before the valley narrowing, and equal or smaller after it, which seems to support the above explanation.

(*b*) *Lee vortices*

The representation of the lee vortices is the forecast aspect which has already progressed between Exps. 3 and 4. Figure 22 now presents a comparison of the Lannemezan sodar simulation between Exps. 4 and 5, at 15 UTC, the hour when the vortices were more intense. The improvement is spectacular for the seven models whose topography has been changed from Exp. 4 to Exp. 5. For three of them (EMC, MC2 and UKMO) a reversed wind (signature of the lee vortices pair) appears in Exp. 5. For two of them (COAMPS, HIRLAM) the southerly wind is strongly reduced, and for the last two models (BOLAM, LAMBO) the wind profile remains the same, but they were already correctly simulating the reversed wind in Exp. 4. On the whole, eight out of eleven models have been able to reproduce a reversed wind at the sodar location with an envelope orography together with an effective roughness length. In fact, the surface wind fields indicate that lee vortices are present in all models but not always with the right location or the right extension.

The RMS error can be calculated from the sodar measurements. Its time evolution for the wind direction is presented on Fig. 23. Because of the coherence of the observed flow the standard deviation of error is quasi-null, therefore bias and RMS are very close. One can recall that the wind direction is not computed when the wind is too weak, the RMS is then set to zero. The difference between the scores for Exps. 4 and 5, is that the big errors in direction begin after 12 UTC in Exp. 4 and at 6 or 9 UTC for Exp. 5. These bad scores for the flow direction signify, in fact, that in some models the lee vortices circulation appears too early. This error may be reduced further in time, when the reversed wind appears in the observed wind field and so coincides with the simulation. This behaviour can be illustrated by the MC2 model. One can notice that in Exp. 4 the ALADIN model seems to reproduce the same evolution, which is not surprising since this model already has an envelope orography in Exp. 4.

In both experiments the maximum error is still at 18 UTC, the prescribed configuration of the models for experiment 5 does not allow better reproduction of the vortices evolution between 15 and 18 UTC. Neither does it reproduce the correct height which can be evaluated at 15 UTC by a wind profiler at Lannemezan around 2000 m. Only two models reproduce the vortices as high as they are (one in each of Exps. 3 and 4).

(*c*) *Mountain wave*

The scores against the aircraft measurements are worse, on average, than for the previous two experiments. For the lower legs the mean RMS of the models is about 1 m s^{-1} bigger for the wind than in Exp. 4. The reason for this degradation is obvious from Fig. 24, since, on the whole the wave amplitude is higher in Exp. 5 than in the previous experiments (cf. Fig. 13). The increase in the height of the mountain was expected to enhance the blocking, which seems to be the case, but it has also lead to the

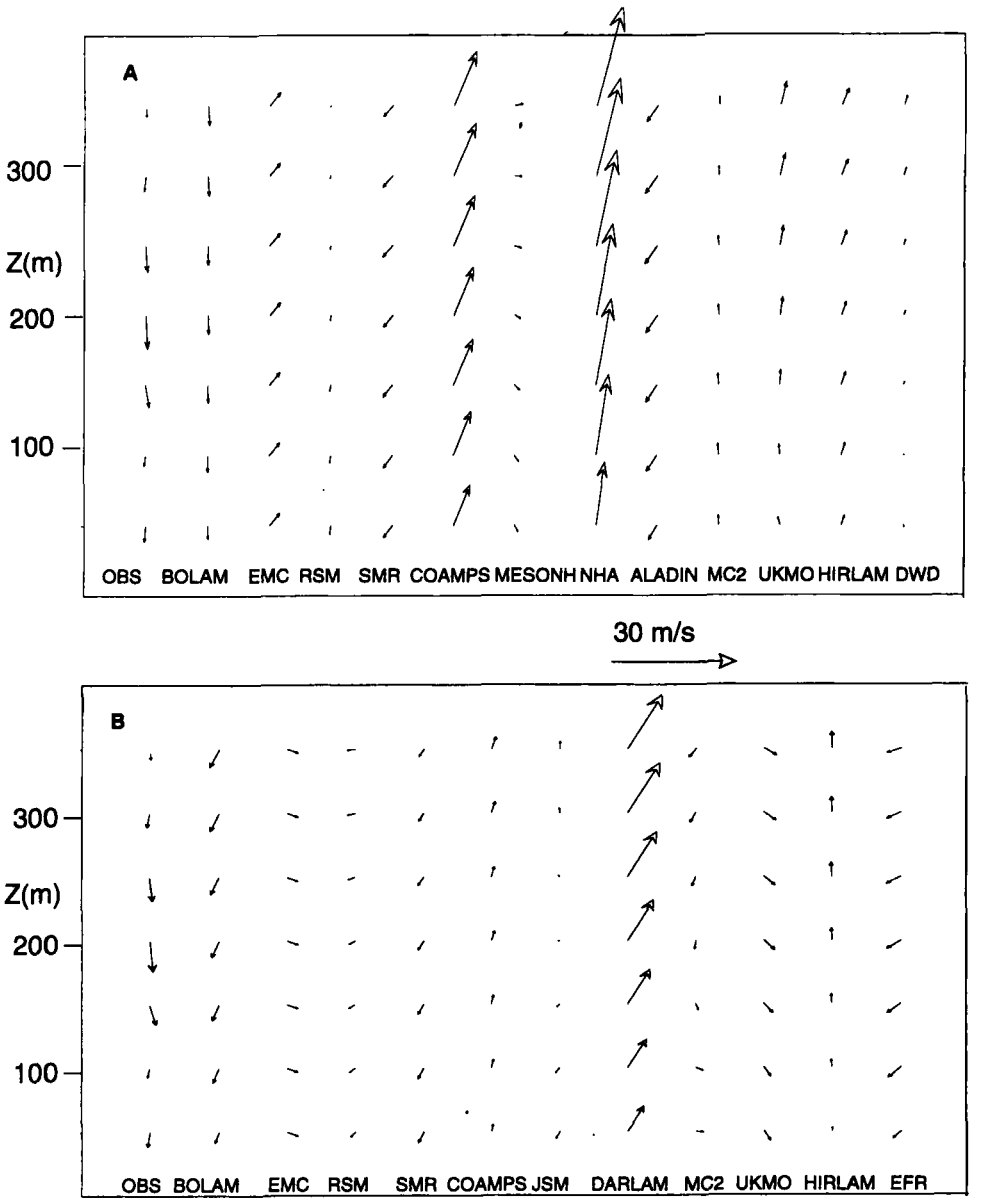

Figure 22. Comparison between model results and sodar measurements, for the horizontal wind, on the first 350 m above Lannemezan at 15 UTC. (A) for Exp. 4; (B) for Exp. 5. (This diagram is slightly horizontally stretched in comparison with the above one.)

enhancement of the mountain-wave amplitude. This stresses the non-linear character of this type of flow.

It has been demonstrated in recent works (Mesinger *et al.* 1996; Georgelin *et al.* 1994) and in section 3(c) that the use of a large (effective) roughness length reduces the wave amplitude and improves the forecast. Here the reference roughness does not seem to be high enough to compensate the wave enhancement due to the envelope topography.

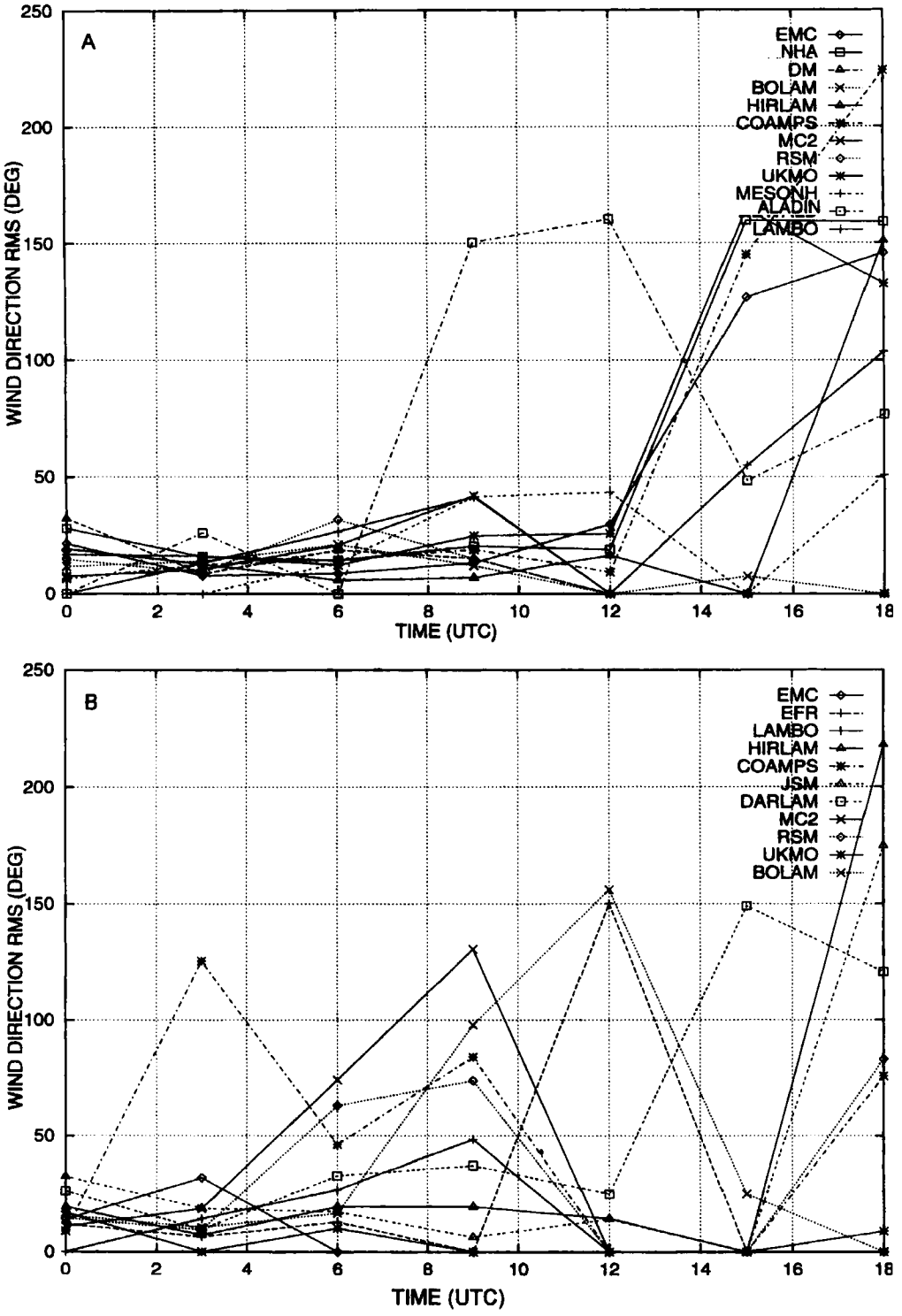

Figure 23. Time evolution of the RMS against observations of wind direction by the Lanemezan sodar. (A) Exp. 4; (B) Exp. 5.

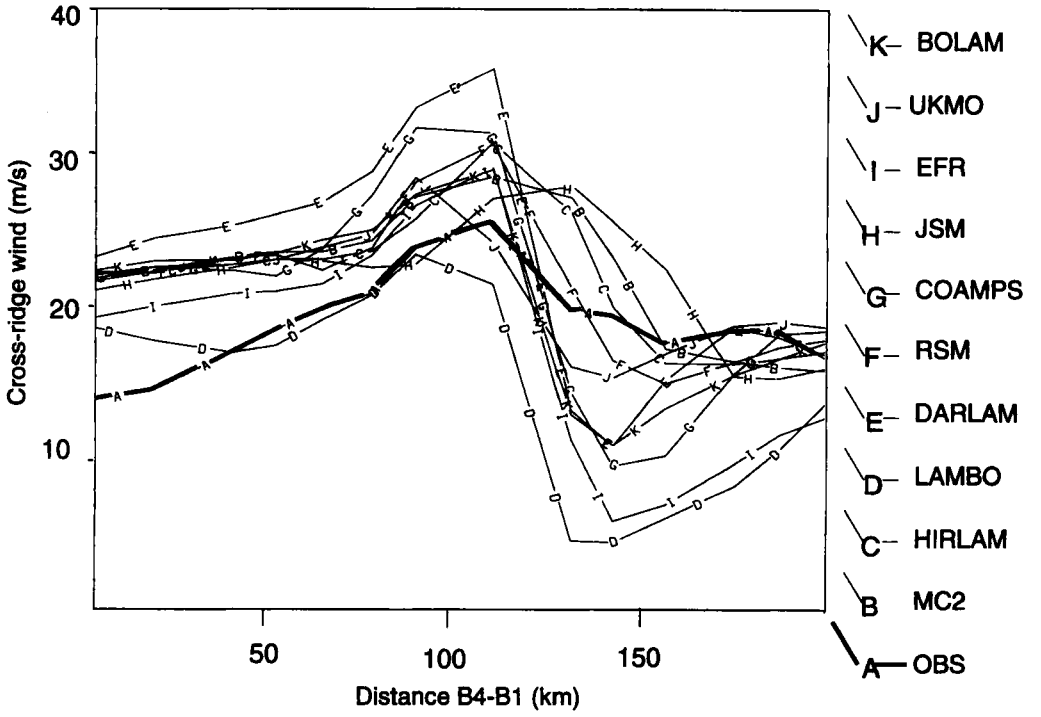

Figure 24. Observed (thick line) and simulated cross-ridge component of the wind, along the 545 hPa leg, for Exp. 5.

(*d*) *Pressure drag*

Experiment 5 is the most homogeneous of all three experiments (same model configuration, same forcing) but its drag (Fig. 25) appears to be more scattered, mostly in the first hours. It can also be noted that the mean of the models is lower than in Exp. 4 (as an exception the too strong drag of the COAMPS model can probably be explained by the fact that the topography was spuriously truncated at the summit). The main improvement between Exps. 4 and 5 occurs with the lee vortices forecast which may explain the drag behaviour. When the lee of a mountain evolves towards a pair of lee vortices, in the central part of the obstacle the wind weakens, then reverses, and finally forms the return current common to the two lee vortices (see Fig. 4). As a consequence of the wind becoming weak or reversed* the pressure will increase downwind of the mountain, and thus the pressure gradient across the ridge, which is the source of the drag, is reduced. This is probably the explanation for the drag decrease of some models, although it has to be remembered that there was no aircraft observation below 615 hPa. The link between the onset of lee vortices and the pressure drag decrease was also noticed in Schär and Duran (1997).

For this experiment it can be confirmed that the drag is not sensitive to the wave variations since it has been shown above that the wave amplitude was excessive in Exp. 5. The fact that vortices appear too early in some simulations is confirmed by the weak values of the drag at 06 or 09 UTC. The largest scattering of the model drag is at 03 UTC; later the models are in closer agreement. Most of the models had to have

* Because it advects colder air.

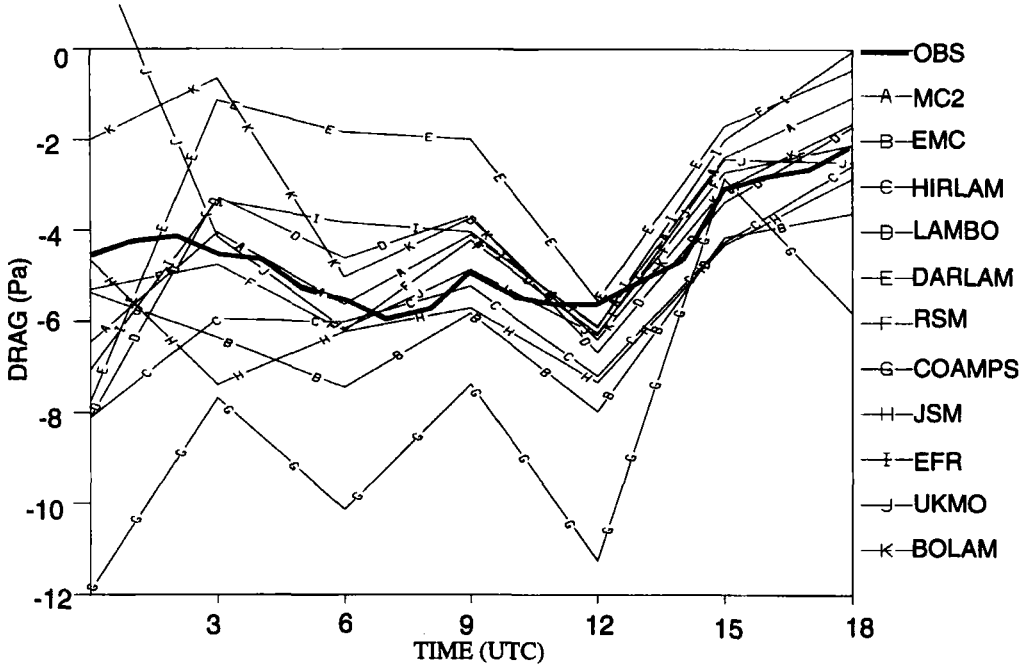

Figure 25. Time evolution of the observed (thick line) and simulated pressure drag for Exp. 5.

their set up changed significantly to participate in Exp. 5; the spin-up of these models could take longer and thus explain the big scattering at 03 UTC.

(*e*) *Discussion*

On the whole the prescribed configuration has not been able to improve the forecast of the IOP3. The only positive action of the envelope orography parametrization has been to favour the appearance of the lee vortices. But the wake vorticity often develops too early. One can notice that an envelope may not be necessary to get the correct wake, since the BOLAM model has succeeded in its simulation in Exp. 4. Some effects of this type of relief representation are counter-intuitive:

- The local wind intensity has not been enhanced by the expected stronger blocking due to the higher mountains; rather it has slightly decreased. Indeed, it seems that the blocking has been enhanced, but the detail of the topography deteriorated, and this aspect may be as important as the height of the summit for the local wind simulation.
- The higher mountains enhance the blocking but at the same time increase the mountain wave amplitude, which again amplifies the gap between the simulated waves and those observed. The effective roughness length has the opposite effect, and could have compensated for this if the provided values of roughness were large enough. Note, for instance, that in Table 2 the EFR, MC2, and UKMO models have stronger roughness lengths than the others (around 20 m).

The drags comparison confirms the existing link between the pressure drag calculated on a section at the centre of the ridge and the wake vortices circulation. The pressure drag is reduced when the return current of the vortices is enhanced.

Generally speaking the use of an envelope orography does not seem to be able to improve the forecast at the mesoscale.

6. SUMMARY

The COMPARE/PYREX exercise has emphasized the fact that the orography representation is still not sufficiently close to reality for accurately forecasting an orographic flow at the mesoscale.

- The discretized mountain does not create enough blocking at low level which results in the local winds intensity being too weak.
- The model topography does not slow down the atmosphere enough, which is why the mountain wave is too strong.

Although the quality of the topographic forcing is preponderant, the study also shows that at the mesoscale an improvement of the large-scale forcing may ameliorate the wake simulation and prevent the simulated waves from departing too much from reality.

The pressure drag was quite correctly reproduced by the majority of the models but the results suggest that it is more sensitive to the lee vortices circulation than to the mountain wave because the minima of this drag are in the return current of the lee vortices. The recent work of Olafsson and Bougeault (1996) reveals that the maximum steepening of the wave is found rather in both sides of the axis of symmetry for a flow similar to the IOP3. It suggests that the pressure drag should be measured on both sides of the central section where it is likely to be the strongest and possibly free of the influence of vortices.

The exercise has also allowed exploration of two parametrizations, the aim of which is to improve the representation of topography in models, since this is still inadequate with a mesh of 10 km, as aforementioned. The impact of an effective roughness length parametrization is to improve the wave simulation, thus confirming some recent work. For the other features of the flow it was not possible to isolate the effect of this parametrization. The impact of an envelope orography has been studied in a more complete way. Its use is curiously without positive effect for the local wind forecast; its more spectacular action is to make strong lee vortices appear in all models, but the balance is not necessarily positive since these vortices often appear too early. An adverse effect of the envelope for this type of flow is also to enhance the wave amplitude. All in all, an envelope orography does not seem an appropriate way to improve the forecast at the mesoscale. It has to be kept in mind that the envelope orography parametrization has been validated by giving the right pressure drag, but the conclusions of the present exercise concerning the drag rather suggest that a correct simulation of the drag may not be sufficient to validate a parametrization.

The COMPARE experiment results emphasize the way a parametrization should be working in order to improve the forecast. The ideal parametrization must be able to increase the blocking at low level without enhancing the wave and without modifying the topographic details. Even with a huge roughness the mountain wave is still too intense, but the value of roughness cannot be increased indefinitely. An effective roughness length does not seem able to significantly increase the local winds. It acts more on the intensity of blocking than on the depth of blocking which determines the quantity of air going around the ridge. A solution may be found with the new parametrization of Lott and Miller (1997) where the low-level drag, a function of the subgrid-scale topography, is distributed on all model levels where the height is below the

real relief. In the same way Masson and Bougeault (personal communication) propose to enhance the production of turbulent kinetic energy and the mixing length to represent the subgrid relief contribution, on a height of twice the standard deviation of topography. A silhouette orography is another alternative which seems to conserve of the topographic detail more than the envelope, but the enhancement of the mountain height will probably lead to the same problem as the envelope. The progress in lee vortices simulation is probably linked to progress in blocking and wave representation. The forecast of the lee eddies evolution between 15 and 18 UTC might have failed because of the small size of the phenomenon in respect to the mesoscale.

ACKNOWLEDGEMENTS

The second COMPARE exercise was made possible by the participation of a large number of institutes.

- The PYREX experiment was funded by Météo-France, the Instituto Nacional de Meteorología (Spain), the Institut National des Sciences de l'Univers (ARAT, PAMOS and PAMOY programmes), the Centre National d'Etudes Spatiales, Electricité de France, Région Midi-Pyrénées, and the Deutsche Forschungsanstalt für Luft und Raumfahrt.
- Datasets distributed were prepared at CNRM by B. Pouponneau, G. Jaubert, J. D. Gril, R. Bubnova.
- Atmospheric Environment Service (RPN) built the large-scale data base (J. Caveen) and helped to fine tune the domains A and B (A. Staniforth, B. Bilodeau, C. Chouinard)
- ECMWF allowed use of its reanalysis (A. Hollingsworth)
- Many participants helped by pointing to errors in the datasets
- The CNRM supported the evaluation study with manpower and funding (D. Cariolle)
- WMO supported the Workshop (F. Delsol)

REFERENCES

Benech, B., Koffi, E., Druilhet, A., Durand, P., Bessemoulin, P., Campins, J., Jansa, A. and Terliuc, B. 1998 Characteristics of local flows around the Pyrénées in view of PYREX experiment data. I: Analysis of the pressure and wind fields and experimental assessment of the applicability of the linear theory. *J. Appl. Meteorol.*, **37**, 32–52

Benoit, R., Côté, J. and Mailhot, J. 1989 Inclusion of a TKE boundary layer parameterization in the Canadian Regional Finite Element Model. *Mon. Weather Rev.*, **117**, 1726–1750

Benoit, R., Desgagné, M., Pellerin, P., Pellerin, S., Chartier, Y. and Desjardins, S. 1997 The Canadian MC2: a semi-Lagrangian semi-implicit wideband atmospheric model suited for finescale process studies and simulation. *Mon. Weather Rev.*, **125**, 2382–2415

Bessemoulin, P., Bougeault, P., Genoves, A., Jansa Clar, A., and Puech, D. 1993 Mountain pressure drag during PYREX. *Beitr. Phys. Atmos.*, **66**, 305–325

Black, T. L. 1994 The new NMC mesoscale model: Description and forecast examples. *Weather and Forecasting*, **9**, 265–278

Bougeault, P., Beau, I. and Stein, J. 1992 'Validation of meteorological models and parameterization with observations of the PYREX field experiment'. Pp. 247–285 in Proceedings of Validation of models over Europe, 7–11 September 1992, ECMWF, Shinfield, Reading, RG2 9AX, UK

Bougeault, P., Jansa, A., Attié, J. L., Beau, I., Benech, B., Benoit, R., Bessemoulin, P., Caccia, J. L., Campins, J., Carissimo, B., Champeaux, J. L., Crochet, M., Druilhet, A., Durand, P., Elkhalfi, A., Flamant, P., Genoves, A., Georgelin, M., Hoinka, K. P., Klaus, V., Koffi, E., Kotroni, V., Mazaudier, C., Pelon, J., Petitdidier, M., Pointin, Y., Puech, D., Richard, E., Satomura, T., Stein, J. and Tannhauser, D. 1993 The atmospheric momentum budget over a major atmospheric mountain range: first results of the PYREX program. *Annales Geophysica*, **11,** 395–418

Bougeault, P., Jansa Clar, A., Benech, B., Carissimo, B., Pelon, J. and Richard, E. 1990 Momentum budget over the Pyrénées: The PYREX experiment. *Bull. Am. Meteorol. Soc.*, **71,** 806–818

1997 PYREX: A summary of findings. *Bull. Am. Meteorol. Soc.*, **78,** 637–650

Bubnová, R., Hello, G., Bénard, P. and Geleyn, J. F. 1995 Integration of the fully elastic equation cast in the hydrostatic pressure terrain following coordinate in the framework of the ARPEGE/ALADIN NWP system. *Mon. Weather Rev.*, **123,** 515–535

Buzzi, A., Fantini, M., Malguzzi, P. and Nerozzi, F. 1994 Validation of a limited area model in cases of Mediterranean cyclogenesis: Surface fields and precipitation scores. *Meteorol. Atmos. Phys.*, **53,** 137–153

Campins, J. A., Jansà, A., Benech, B. and Koffi, E. 1995 PYREX observation and diagnosis of the Tramontane wind. *Meteorol. Atmos. Phys.*, **56,** 209–228

Chouinard, C., Mailhot, J., Mitchell, H. L., Staniforth, A. and Hogue, R. 1994 The Canadian Regional Data Assimilation System: Operational and Research Applications. *Mon. Weather Rev.*, **122,** 1306–1325

Cullen, M. J. P. and Davies, T. 1991 A conservative split-explicit integration scheme with 4th order horizontal advection. *Q. J. R. Meteorol. Soc.*, **117,** 993–1002

Durran, D. R. 1990 Mountain wave and downslope winds. Atmospheric process over complex terrain, meteorological monographs. *Amer. Meteorol. Soc.*, **23**(45), 59–81

Eliassen, A. and Palm, E. 1960 On the transfer of energy in stationary mountain waves. *Geophys. Norv.*, **22,** 1–23

Georgelin, M., Richard, E., Petitdidier, M. and Druilhet, A. 1994 Impact of subgrid scale orography parameterization on the simulation of orographic flows. *Mon. Weather Rev.*, **122,** 1509–1522

Georgelin, M., Richard, E. and Petitdidier, M. 1996 The impact of a diurnal cycle on a low Froude number flow observed during the PYREX experiment. *Mon. Weather Rev.*, **124,** 1119–1131

Gyakum, J. R., Chouinard, C., Staniforth, A., Béland, M., Benoit, R., de Elia, R., Drummond, F., Kuo, Y. H., Lalaurette, F., Laprise, R., Leslie, L., Lin, H., Mailhot, J., Merilees, P. E., Tyler, R. and Wintels, W. 1995 First COMPARE Workshop 3–5 October 1994, Montreal, Quebec, Canada *Bull. Am. Meteorol. Soc.*, **78,** 1209–1218

Gyakum, J. R., Carrera, M., Zhang, D. L., Miller, S., Caveen, J., Benoit, R., Black, T., Buzzi, A., Chouinard, C., Fantini, M., Folloni, C., Katzfey, J. J., Kuo, Y. H., Lalaurette, F., Low-Nam, S., Mailhot, J., Malguzzi, P., McGregor, J. L., Nakamura, M., Tripoli, G. and Wilson, C. 1996 A regional model intercomparison using a case of explosive oceanic cyclogenesis *Weather and Forecasting*, **11,** 521–543

Hodur, R. M. 1997 The Naval Research-Laboratory Coupled Ocean/Atmosphere Mesoscale Prediction System. *Mon. Weather Rev.*, **125,** 1414–1430

Hong, S. Y. and Pan, H. L. 1996 Non local boundary layer vertical diffusion in a medium range forecast model. *Mon. Weather Rev.*, **124,** 2322–2339

Ikawa, M. and Saito, K. 1991 'Description of a non-hydrostatic model developed at the Forecast Research Department of the MRI'. Tech. Rep. of the MRI, No. 28

Janjic, Z. I. 1994 The step-mountain eta coordinate model: Further developments of the convection, viscous sublayer and turbulence closure schemes. *Mon. Weather Rev.*, **122,** 927–945

Juang, H. M. H. and Kanamitsu, M. 1994 The NMC nest regional spectral model. *Mon. Weather Rev.*, **122,** 3–26

Källén, E. (ed.) 1996 HIRLAM documentation manual. System 2.5 (available from Norrköping, Sweden)

Koffi, E., Benech, B., Stein, J. and Terliuc, B. 1997 Characteristics of local flows around the Pyrénées in view of PYREX experiment data. II: Solution of an advanced linear theory model compared to field measurements. *J. Appl. Meteorol.*, **37,** 53–71

Lafore, J. P., Stein, J., Asencio, N., Bougeault, P., Ducrocq, V., Fischer, C., Héreil, P., Mascart, P., Masson, V., Pinty, J. P., Redelsperger, J. L., Richard, E. and Vilá-Guerau de Arellano, J. 1998 The Meso-NH Atmospheric Simulation System. I: adiabatic formulation and control simulations. *Ann. Geophys.*, **16,** 90–109

Lott, F. and Miller, M. J. 1997 A new sub-grid scale orographic drag parameterization: its formulation and testing. *Q. J. R. Meteorol. Soc.*, **123,** 101–127

Mailhot, J., Sarrazin, R., Bilodeau, B., Brunet, N. and Pellerin, G. 1997 Development of the 35 km version of the Canadian Regional Forecast System: *Atmos.–Ocean*, **35,** 1–28

Majewski, D. 1997 Operational regional prediction. *Meteorol. Atmos. Phys.*, **63,** 89–104

Masson, V. and Bougeault, P. 1996 Numerical simulation of a low-level wind created by complex orography: A Cierzo case study. *Mon. Weather Rev.*, **124,** 701–715

McGregor, J. L. 1993 Economical determination of departure points from semi-Lagrangian models. *Mon. Weather Rev.*, **121,** 221–230

McGregor, J. L. and Walsh, K. 1994 Climate change simulations of Tasmanian precipitation using multiple nesting. *J. Geophys. Res.*, **99,** 20889–20905

Mesinger, F., Janjic, Z. I., Nickovic, S., Gavrilov, D. and Deaven, D. G. 1988 The step mountain coordinate: Model description and performance for cases of Alpine lee cyclogenesis and for a case of Appalachian redevelopment. *Mon. Weather Rev.*, **116,** 1493–1518

Mesinger, F., Wobus, R. L. and Baldwin, M. E. 1996 Parameterization of form drag in the eta model at NCEP. Pp. 324–326 in preprints of the AMS 11th conference on numerical weather prediction, Norfolk, VA, USA. (Available from the American Meteorological Society, Boston, USA)

Olafsson, H. and Bougeault, P. 1996 Non-linear flow past an elliptic mountain ridge. *J. Atmos. Sci.*, **53,** 2465–2489

1997 The effect of rotation and surface friction on orographic drag. *J. Atmos. Sci.*, **54,** 193–210

Paccagnella, T., Tibaldi, S., Buizza, R. and Scoccianti, S. 1992 High resolution numerical modeling of convective precipitation over northern Italy. *Meteorol. Atmos. Phys.*, **50,** 143–163

Saito, K. 1994 A numerical study of the local downslope wind "Yamaji-kaze" in Japan. III: Numerical simulation of the 27 September 1991 wind-storm with a non-hydrostatic multi-nested model. *J. Meteorol. Soc. Jpn*, **72,** 301–329

Schär, C. and Durran, D. R. 1997 Vortex formation and vortex shedding in continuously stratified flows past isolated topography. *J. Atmos. Sci.*, **54,** 534–554

Segami, A., Kurihara, K., Nakamura, H., Ueno, M., Takano, I. and Tatsumi, Y. 1989 Operational mesoscale weather prediction with Japan Spectral Model. *J. Meteorol. Soc. Jpn*, **67,** 907–924

Smith, R. B. 1989 Hydrostatic airflow over mountains. *Adv. Geophys.*, **31,** 1–41

Smith, R. B. and Grubišić, V. 1993 Aerial observation of Hawaii's wake. *J. Atmos. Sci.*, **50,** 3728–3750

Smolarkiewicz, P. K. and Rotunno, R. 1989 Low Froude number flow past three-dimensional obstacles. I: Baroclinically generated lee vortices. *J. Atmos. Sci.*, **46,** 1154–1164